3

Silver and Gold Nanoparticles on Sol-Gel TiO_2, ZrO_2, SiO_2 Surfaces: Optical Spectra, Photocatalytic Activity, Bactericide Properties

Anna Eremenko[1], Natalia Smirnova[1], Iurii Gnatiuk[1], Oksana Linnik[1], Nadezhda Vityuk[1], Iuliia Mukha[1] and Aleksander Korduban[2]
[1]*Chuiko Institute of Surface Chemistry of National Academy of Sciences of Ukraine,*
[2]*Kurdyumov Institute of Metallophysics of National Academy of Sciences of Ukraine,*
Ukraine

1. Introduction

Development of new nanomaterials with metal nanoparticles (Ag, Au, Cu, Rh, Pd, *etc.*) deposited on oxide surfaces, embedded within pores or encapsulated in its matrices have gained much attention in material science because of expanding applications of such composites in optics, medical diagnostics, analytical chemistry, catalysis, photocatalysis *etc*. The most widely used catalyst is titanium dioxide. Titania effective properties could be improved by mixing with other oxides (ZrO_2, SiO_2, ZnO) that act as additives to control structure-sorption, optical and electronic properties. Incorporation of metal nanoparticles into a solid matrix of titania enhances their quantum efficiency (Kim et al, 2001; Alberius, 2002). Semiconductor-metal composite nanoparticles have been shown to facilitate charge rectification in the semiconductor nanostructures that is beneficial for maximizing the efficiency of photocatalytic reactions (Kamat, 2003, Subramanian et al, 2001). The metal NPs, being adsorbed or incorporated into titania matrix, modify the interface and/or alter the pathways with which photogenerated charge carriers undergo recombination or surface reactions. Metal nanoparticles embedded in dielectric matrixes are promising composite materials for optical applications as systems with enhanced third-order electronic susceptibility $\chi^{(3)}$ [SiO_2-ZrO_2-Ag]. Aggregation and reshaping of metal nanoparticles and other processes occurring at the nanometal/porous matrix interfaces on preparation or post-reaction treatments, as well as mutual influence of their electronic structures, physical or chemical interactions of phases, affect many characteristics of nanocomposites (Chan et al, 2004; Epifani et al, 2000; Gonella et al, 1999; He J. et al, 2002; He C. et al, 2002; Liz-Marzan et al, 1996; Kelly et al, 2003; Kreibig and Vollmer, 1995; Shacham et al, 2004; Shter et al, 2007; Song et al, 2005).

There are hundreds publications devoted to the fabrication techniques of nanosized titania-based photocatalyst and the properties description of obtained materials. The methods of synthesis including sol-gel process with thermoinduced (Antonelli & Ying, 1995), photo- or chemical reduction of metal ions deposited on the TiO_2 surface (Smirnova et al, 1992), as well as combination of ion-exchange and reduction process (Gnatyuk, 2005) were proposed for preparation of films containing small particles of metals and semiconductor (Kim et al, 2001; Alberius, 2002; Antonelli & Ying, 1995; Smirnova et al, 1992; Gnatyuk et al, 2005).

The sol-gel techniques are most effective and popular on preparation of metal/oxide or metal/organics nanocomposites (Chan et al, 2004; Epifani et al, 2000; Gonella et al, 1999; He J. et al, 2002; He C. et al, 2002; Liz-Marzan et al, 1996; Kelly et al, 2003; Kreibig and Vollmer, 1995; Shacham et al, 2004; Shter et al, 2007; Song et al, 2005; Traversa et al, 2001). However it is not analyzed in the literature the interrelation of the synthetic conditions and physico-chemical properties of obtained materials, and hence the recommendations for the preparation of effective stable photocatalyst based on titania films and modified with small amount of noble metal nanoparticles (NPs).

In this work we present improved photo- thermochemical production of TiO_2, ZrO_2, ZnO and SiO_2,- metal functional films, as well as binary and ternary oxide composites via template assisted sol-gel method and doped with Ag and Au nanoparticles (NPs). Metal NPs have been synthesized by photochemical, chemical or thermal reduction of appropriate ions and embedded into oxide matrices via adsorption from their colloids or by the direct thermoreduction of metal ion/oxide composition with attempt to enhance their photocatalytic (M/TiO_2-based composites) and bactericide (M/SiO_2 composites) activity. Investigations of optical properties, XPS, surface morphology, electronic structure and photocatalytic activity have been performed.

2. Experimental part

All reagents were used as received. Template sol-gel method was applied for preparation of mesoporous silica, titania and zirconia films at glass and silicon substrates. Detailed procedure for the films synthesis with embedded noble metal nanoparticles is described in (Krylova et al, 2009). To form Ag and Au nanoparticles embedded within the oxide films, an appropriate amounts of $AgNO_3$ or $HAuCl_4$ were added to the precursor sols. Concentration of the Ag^+ ions was varied from 1 to 30 at.% and Au^{3+} ions from 1 to 7 at.% compared to molar concentration of alkoxides.

For film deposition onto glass or silicon wafers, dip-coating technique was utilized. After deposition of the film, gelation and gel ripening, it was dried in air at room temperature for 2 h (dried samples). Then the dried films were sintered in a furnace at a heating rate $\beta = 2\ ^oC/min$ to 250 ^oC, and at $\beta = 0.25\ ^oC/min$ from 250 to 350 ^oC. Template burns out at these temperatures and this process should be carefully carried out for keeping the ordered porous structure of the oxide film/Ag, Au nanoparticles. Then temperature was elevated to 500, 550 and 600 ^oC at $\beta = 3\ ^oC/min$ and the systems were kept at a certain temperature for 3 h.

Zinc ions modified titanium dioxide mesoporous films were synthesized by sol-gel method. The film covering on the clean glass substrate was performed by means of dip-coating techniques. The generation of the gold particles in the film structure was performed by different procedures. The first two methods were grounded on the admixing of (3 mol %) tetrachloroauric ions during titanium and zinc sol formation. Particularly, the first one consists of the drying of every layer at 60 ^oC for 30 min and UV light action for 10 min. The slow heating to 500 ^oC for 6 hours was done ($TiO_2/ZnO/Au_{ph\text{-}t}$, colored in pink). The second way was to treat every layer at 200 ^oC for 10 min with final irradiation by UV light for 30 seconds and annealing at 500^o C for 2 h ($TiO_2/ZnO/Au_t$, colored in blue). The third method is based on the adsorption process. Previously synthesized and calcined (500^o C) Zn^{2+}/TiO_2 film was dip-immersed in tetrachloroauric acid solution adjusted to pH 4 for 30 sec. These films were dried and exposed to UV light for 60 sec. The films were coded as $TiO_2/ZnO/Au_{ads}$ film (colored in dark-blue). Hence, Au^{3+} ions were reduced 1) in the sol of

zinc and titanium metalorganic species; 2) in the sol where crystallization of TiO_2 could take place; and 3) on the surface of anatase doped with zinc ions. A source of UV light was 1000 W middle - pressure mercury lamp. The absorption spectra of the films were recorded by Lambda 35 UV-Vis spectrophotometer (PerkinElmer) in the range of 200-1000 nm. It must be noted that the duration of film irradiation was experimentally established, no change in the SPR band intensity was observed after longer irradiation exposure and the reproducibility of the film synthesis was achieved for all three procedures.

The solutions of tetracycline hydrochloride (Aldrich) were prepared by the dissolving of an appropriate amount of the antibiotics in freshly distilled water. The film was immersed in 40 ml of $2 \cdot 10^{-5}$ mol/L (9.6 mg/L) TC solution until complete adsorption in the dark occurred and then irradiated by 1000 W middle-pressure mercury lamp. The reaction temperature was kept constant (25 ^{o}C) during irradiation. The change of the absorption spectra was recorded by Lambda 35 UV-vis spectrophotometer (PerkinElmer). The reaction rate was estimated as the pseudo-first order and calculated as a change in the TC absorption intensity at λ=357 mn. (Linnik et al, 2009).

SEM images were registered on SEM LEO-1530. EDS spectra were obtained using Brucker AXS X-ray detector.

XPS spectra were registered on ES-2402 with PHOIBOS-100_SPECS using Mg Kα line of 200 W Mg X-ray tube as a radiation source at 1253,6 eV. Vacuum in a camera maintained at $2 \cdot 10^{-7}$ Pa. The film's size covered on Si wafer was 10x10 mm. The XPS signals were fitted using Gaussian-Newton method.

Photooxidation of Rhodamine B dye aqueous solutions (1x10 -5 mol/l) in the presence of a film with a mass of about 1 mg, was performed in a quartz reactor with water-cooling under vigorous stirring at pH = 6-7. The UV light was provided by a 1000 W low-pressure mercury lamp (λ = 254 nm, P = 2.91×10^{-7} quants/s). The changes of the Rhodamine B concentration were monitored by absorption measurements at 554 nm.

Optical spectra (transmission mode) of the films were recorded using a Lambda UV-Vis (Perkin Elmer) spectrometer.

3. Optical properties of sol-gel films modified by metal nanoparticles

Optical properties of metal nanoparticles containing sol-gel derived films are strongly dependent on the synthesis history of the samples.

Two different routes of synthesis of SiO_2, TiO_2 and ZrO_2 and mixed oxide films modified with Ag and Au nanoparticles that can be described as one-step thermal reduction of metal ions in the inorganic matrix during its sintering and a procedure that includes two stages, namely photoreduction of the metal ions with subsequent thermal treatment of composite films at elevated temperatures have been studied. Both proposed synthesis strategies led us to the formation of metal nanoparticles containing inorganic films but with different optical and surface properties.

3.1 SiO_2, TiO_2 and ZrO_2 films with embedded Ag and Au nanopartiles obtained by thermal - induced reduction

Thermal-induced formation of the metal nanoparticles in the mesoporous silica, titania, zirconia and mixed oxide matrixes during their sintering at temperatures higher than 500 ^{o}C is a result of electron attachment to Ag^{+} and Au^{3+} ions from organic substances of the sol-gel films or their decomposition products. Inorganic SiO_2, TiO_2 and ZrO_2 films

with uniformly distributed Ag and Au nanoparticles and intensive coloration, characteristic for surface plasmon absorption of silver and gold nanoparticles have been obtained when the films doped with different amounts of metal ions were heat treated at elevated temperatures.

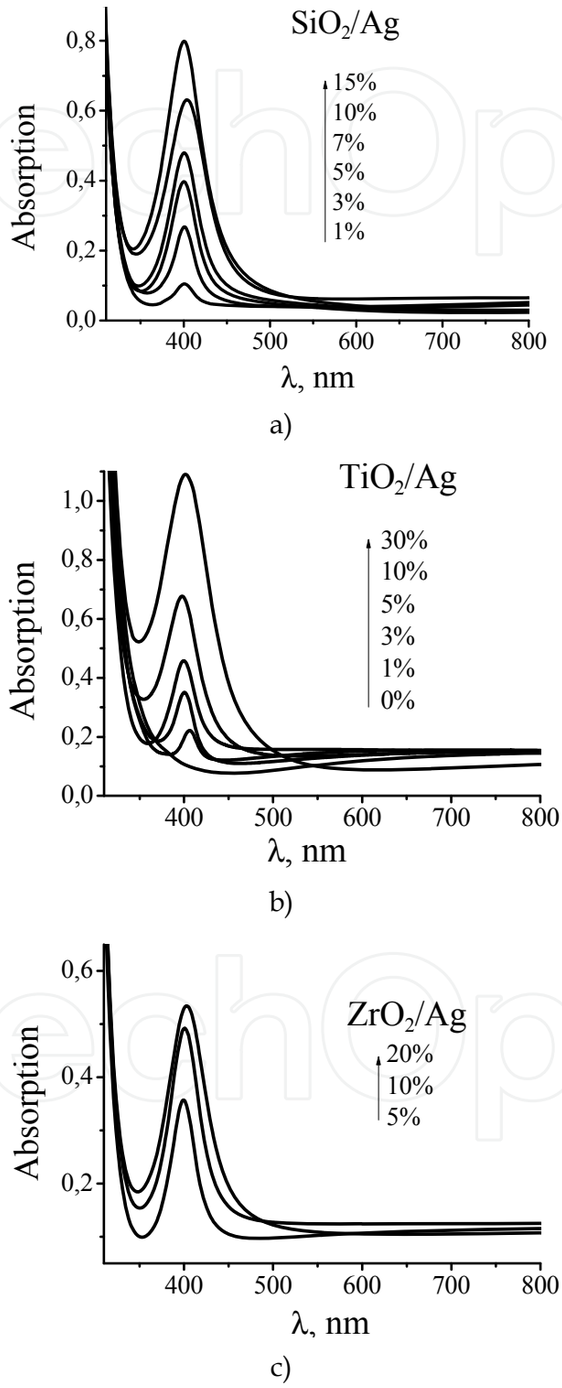

Fig. 1. Absorbance spectra of films sintered at 500 ^{o}C (2 hrs) with increasing Ag^{+} content in the initial sol for a) SiO_2/Ag; b) TiO_2/Ag and c) ZrO_2/Ag.

In the absorption spectra of silica, titania and zirconia films doped with silver ions and sintered at 500 ^oC (Fig. 1), an intensive, symmetric absorption band at around 400 nm appeared due to the silver nanoparticles formation induced by thermal reduction of metal ions as it was described before. The uniform distribution of Ag nanoparticles within the surface and near-surface layers of SiO_2 and TiO_2 films was confirmed by SEM images of the corresponding samples (Fig. 2). The mean particles size of Ag nanoparticles varies depending on the host matrix and is equal to 5-9 nm in the case of silica and 3-5 nm for titania films. We have attributed this change of the particles size of the formed nanoparticles to the differences in crystallinity of the matrixes. Obviously, amorphous structure of silica at 500 ^oC favors continuous movement of silver ions and formed nanoparticles that leads to the larger metal nanoparticles in the final structures.

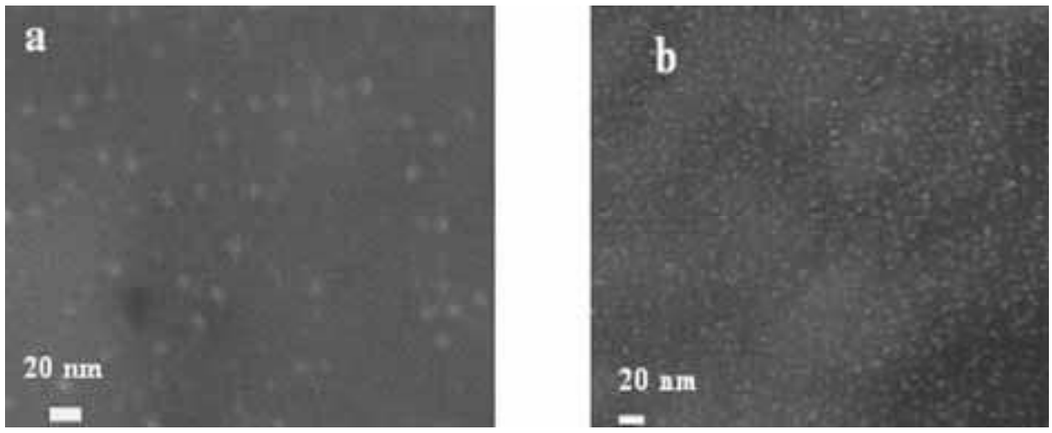

Fig. 2. SEM images of mesoporous films sintered at 500 ^oC: a) SiO_2/Ag 10% and b) TiO_2/Ag 10%.

Elevating of the sintering temperatures of the inorganic matrixes with embedded Ag nanoparticles leads to certain spectral changes in the absorption spectra of the films: shape of the surface plasmon band, position and intensity. These changes depend also on the initial content of the silver ions in the films. Thermal transformations of the absorption spectra of silver nanoparticles containing films depending on the concentration of silver dopant and heat treatment conditions are illustrated in the Fig. 3 for the case of TiO_2 as the host matrix. At low silver content (0.3-5 mol.%) increase of the sintering temperatures up to 550-600 ^oC was accompanied with the decrease of the surface plasmon band intensity and the appearance of new long-wave band at about 470-520 nm for the films with 5 mol.% of silver and heat treated at 600 ^oC.

This effect was attributed to the evaporation of nanosized silver from the outer surface of the films and formation of larger silver particles in the latter case. When SiO_2, TiO_2 and ZrO_2 films were doped with 10 mol.% of silver, elevating of the heat treatment temperatures leads to the increasing of the integral absorbance of the films in the spectral range of absorption of silver nanoparticles, and again, to the appearance of the long-wave band, mentioned before. For the films with further increased silver content up to 30 mol.% only steady increasing of intensity of silver nanoparticles absorption could be noticed. We have concluded that continuous reduction of silver ions takes place compensating evaporation loses of the nanosized silver, when the films with bigger amount of silver ions are subjected to the

elevated sintering temperatures, leading to the increasing of integral absorbance of the films. The formation of the long-wave band in the absorption spectra of the silver nanoparticles containing inorganic films might correspond to the appearance of nonspherical silver particles (Kelly et al, 2003; Link et al, 2001).

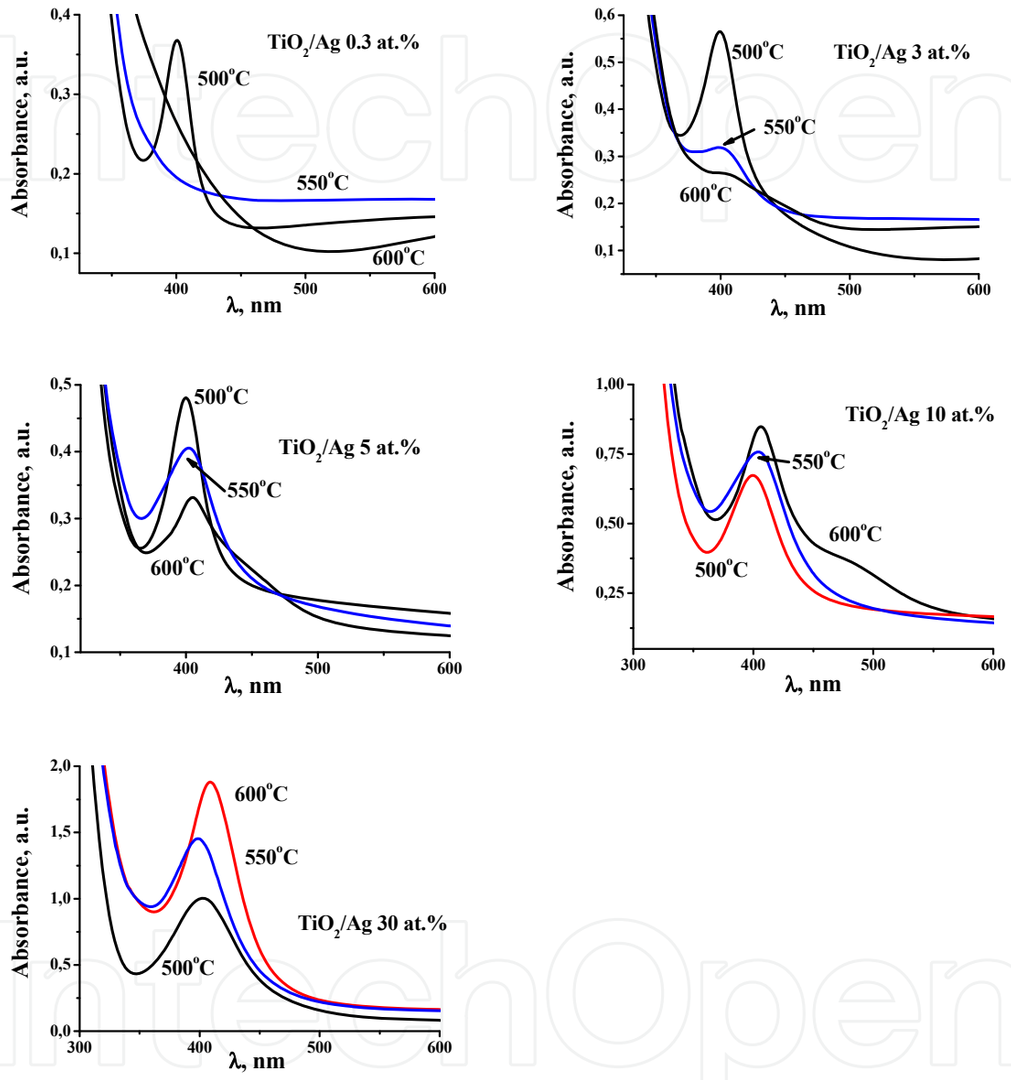

Fig. 3. Evolution of the absorbance of TiO_2/Ag films depending on the silver content and heat treatment temperature.

Thermal-induced formation of gold nanoparticles in the inorganic matrixes starts at lower temperatures due to the differences in thermal stability of the metal ions sources. Chloroauric acid used in the films as Au^{3+} source, is less thermally stable in comparison with silver nitrate. The scheme of thermal transformations of $HAuCl_4$ is presented below:

$$HAuCl_4 \xrightarrow{120°C} AuCl_3 \xrightarrow{185–200°C} AuCl \xrightarrow{290°C} Au$$

Heat treatment of the SiO_2/Au 1% film at temperatures more than 400°C was accompanied with the formation of gold nanoparticles within the silica matrix. The wide surface plasmon band at 535 nm characteristic for Au nanoparticles appeared in the absorption spectrum of the composite film (Fig. 4).

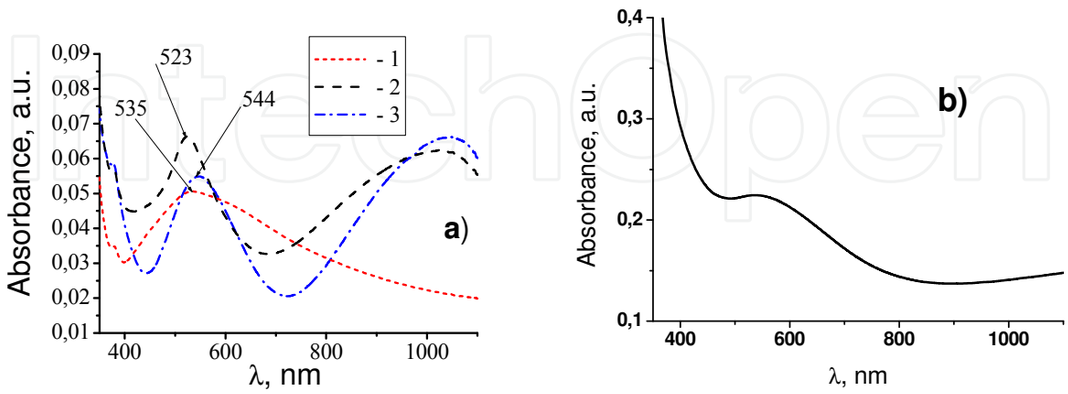

Fig. 4. Absorbance spectra of a) SiO_2/Au 1% film sintered at different temperatures (3 hrs) 1) 400 °C; 2) 450°C; 3) 500 °C and b) TiO2/Au 1% film sintered at 500 °C (2 hrs).

Elevation of sintering temperature of the films up to 450°C caused some blue shift and increase of intensity of the main absorption band of Au nanoparticles (523 nm) with spherical shape and formation of the additional long-wave band at approximately 1000 nm, characteristic for the absorption of the trigonal prism shape gold nanoparticles in accordance with (Huang et al, 2004). Thermal treatment of the SiO_2/Au 1% film at 500°C leads to decrease of intensity and red shift up to 544 nm of the short-wave absorption band of gold nanoparticles with increase of intensity of the long-wave absorption band. We attribute these spectral changes to the growth of spherical and prismatic gold nanoparticles as the result of thermal facilitated movement of the particles.

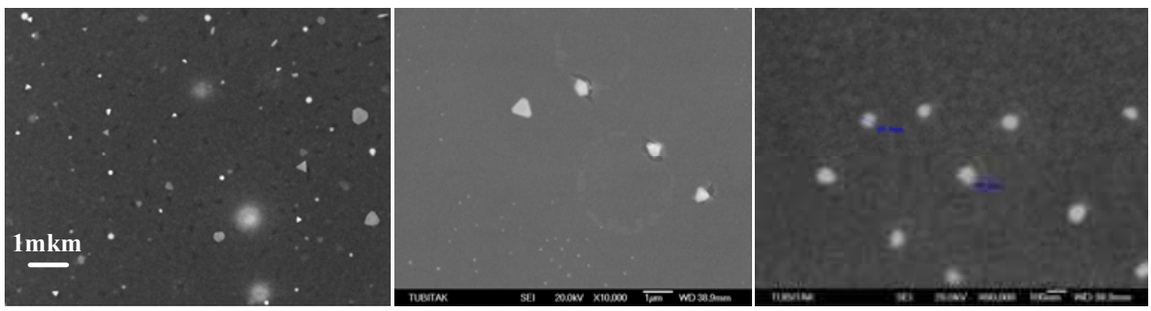

a) b) c)

Fig. 5. SEM images of the mesoporous films with embedded gold nanoparticles a) SiO_2/Au 1% and b, c) TiO_2/Au 1%.

In the SEM images of surface of silica and titania films modified with gold nanoparticles (Fig. 5) we have observed formation of large gold nanoparticles of different shape which conform with the conclusions of analysis of optical spectra of the films. Bimodal particles size distribution was observed for thermally reduced Au nanoparticles in the analyzed host

matrixes with mean particles size in the range of 90-110 nm and 230 nm. Formation of the large trigonal prisms with the size up to 400-500 nm predominantly on the film surface confirms the assumption of the growth mechanism of the particles proposed earlier for silver nanoparticles in SiO_2, TiO_2 and ZrO_2 matrixes (Krylova et al, 2009).
The hydrophilic-hydrophobic interactions between hydrophilic oxide surface (host matrix) and hydrophobic surface of metal nanoparticles will govern metal nanoparticles onto the outer surface of the host. On the other hand, thermal-induced reduction of the metal ions and charged clusters by volatile organics formed during template and organic ligands decomposition/burning out facilitates transfer of reduced atoms, clusters by the gaseous flow onto the outer surface of the films. The other factor – steric hindrance in confined space of the pores, which hinder nanoparticles growth – is much weaker at the outer surface, where the forces of mutual ions/atoms/nanoparticles interactions are smaller than within pores. In other words, particles have more freedom for their diffusion, clusterization and agglomeration (Krylova et al, 2009).

3.2 TiO_2 and TiO_2/ZnO films modified with Ag nanopartiles by photoreduction of metal ions and subsequent thermal treatment

For the photoreduction of metal ions on the surface of inorganic matrix with the aim of formation of metal nanoparticles on it, titanium dioxide was chosen as appropriate one due to its photocatalytic activity. It was observed, that when TiO_2 mesoporous films have been UV irradiated after adsorption of silver ions from the solutions of silver nitrate or silver ammonia complex, photodeposition of nanosized silver islands takes place. This photodeposition process is widely used in literature for the production of novel catalysts, functional surfaces, optical elements, etc. (Sclafani et al, 1997; Subramanian et al, 2001).

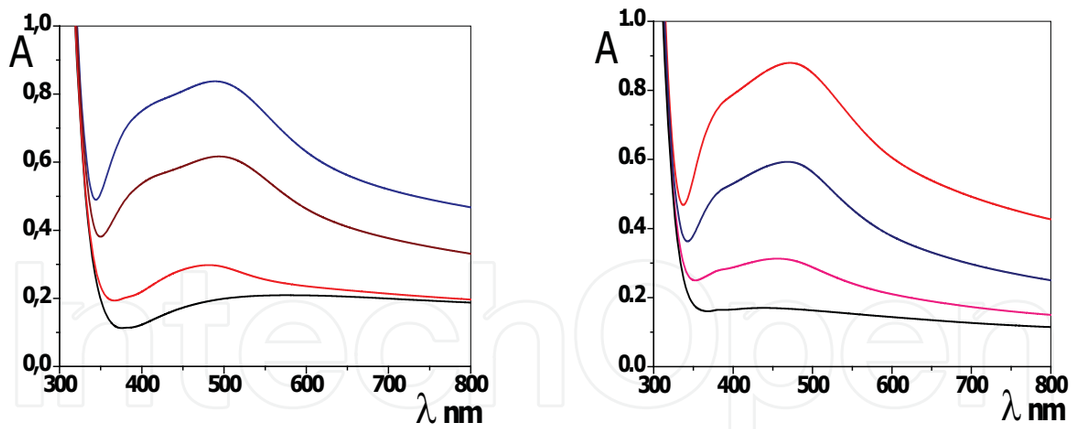

a) b)

Fig. 6. Evolution of absorption spectra of TiO_2 films with photoreduced silver nanoparticles depending on the accumulation of silver NPs during irradiation time when: $AgNO_3$ (a), and $[Ag(NH_3)_2]NO_3$ (b) are used as silver ion sources.

In the absorption spectra of the TiO_2/Ag films with photodeposited silver particles broad complex absorption surface plasmon band of nanosized silver with maxima at 390 and 490 nm was detected. This band corresponds to the fromation of silver particles with broad particles size distribution (Epifani et al, 2000; Lance et al, 2003). In the case of photodeposition of silver nanoparticles from silver ammonia complex $[Ag(NH_3)_2]NO_3$ the

surface plasmon band of silver has more distinct shape with maxima at 390 and 460 nm. The intensity of the band in both cases increases with increasing of the deposited silver content. In addition some maximum displacement towards longer wavelength, characteristic for the agglomeration of the silver particles can be detected.

As the shape and position of the formed silver nanoparticles absorption depends on the silver source used, to control the dispersion of silver particles on the surface of photoactive films, we have decided to incorporate amphoteric zinc oxide into TiO_2 matrix, which sites after leaching in basic solutions (ammonia), may play a role of ion exchange sites for silver complex adsorption and further silver nanoparticles nucleation upon photoreduction and subsequent thermal treatment, as was previously proposed for Mg^{2+} modified wet TiO_2 films by He et al (He J. et al, 2003).

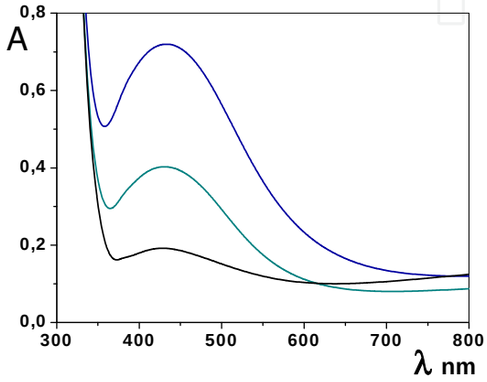

Fig. 7. Evolution of absorption spectra of TiO2/1% ZnO films with photoreduced silver nanoparticles depending on the accumulation ofAg NPs during irradiation when [Ag(NH3)2]NO3 was used as silver ion source.

It was observed, that in the absorption spectra of the UV irradiated TiO_2/ZnO mesoporous films with adsorbed silver ions after ion exchange in silver ammonia complex solutions broad surface plasmon band of nanosized silver with maximum at 440 nm was formed, whereas the band at 390 nm was not observed contrary to the results when silver nitrate was applied. It indicates more uniform silver particles size distribution.

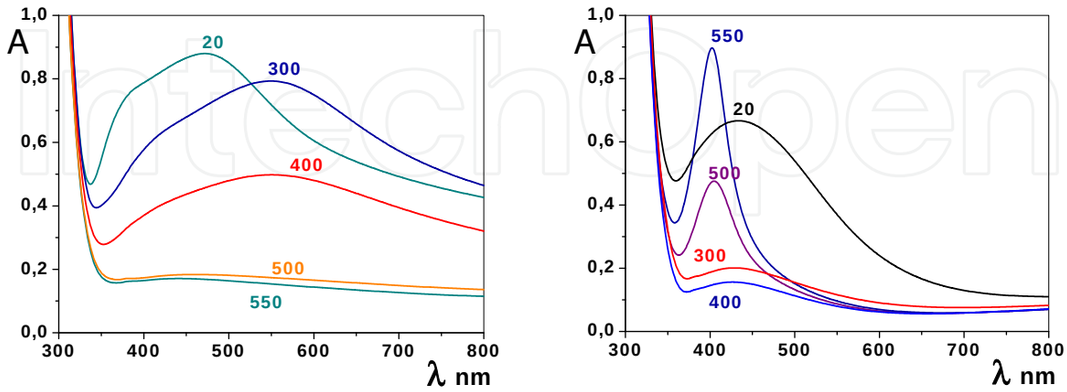

a) b)

Fig. 8. Absorption spectra of TiO_2 (a) and TiO_2/1% ZnO (b) films with photoreduced silver nanoparticles after thermal treatment at different temperatures (indicated near the spectral bands).

Subsequent thermal treatment of the TiO_2 and TiO_2/ZnO films with photodeposited silver caused significant changes in the absorption spectra of the composite films. Red shift and decrease of intensity of the surface plasmon band of nanosized silver was observed for the TiO_2/Ag films upon heating up to 400 ^oC with further complete disappearance of the absorption typical for Ag nanoparticles after film sintering at 500-550 ^oC, that can be attributed to the formation of extremely small silver particles on the film surface and/or partial dissolution of the silver nanodrops in the TiO_2 crystalline matrix (He J. et al, 2003; Krylova et al, 2009).

Different absorption spectra evolution was observed for the TiO_2/ZnO films with photodeposited silver. Surface plasmon band of silver particles disappears at all upon film heating up to 300-400 ^oC whereas after increasing of the sintering temperature of the composite up to 500-550 ^oC distinct intensive absorption band of spherical silver nanoparticles at 400 nm appears in the absorption spectrum of the film.

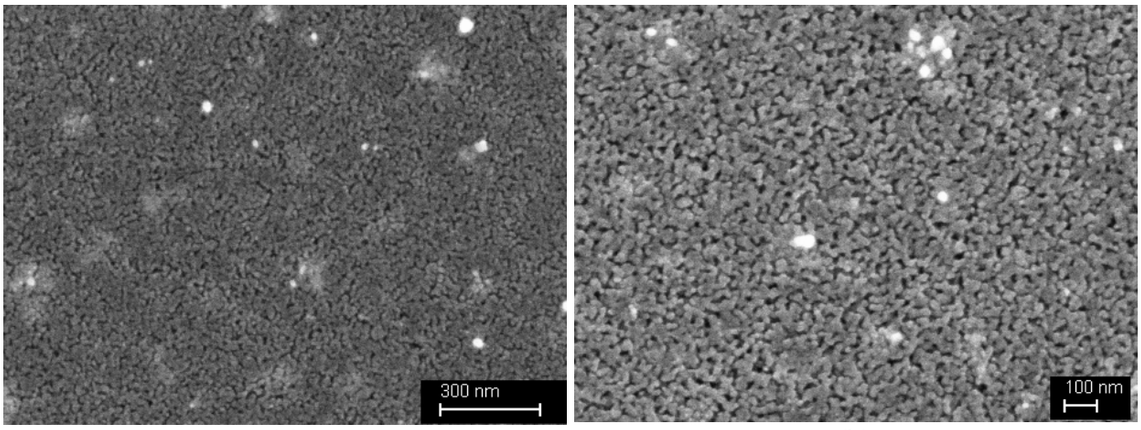

(a) (b)

Fig. 9. SEM images of mesoporous TiO_2 (a) and TiO_2/1% ZnO (b) films with photoreduced silver after thermal treatment at 550^{o}C.

We believe that during ion exchange taking place at the zinc oxide rich sites of the TiO_2 matrix when the latter is being immersed into silver ammonia complex, the sites within the TiO_2 matrix for further nucleation of silver nanoparticles have been appeared.

Uniform distribution of silver nanoparticles over mesoporous TiO_2 and TiO_2/ZnO surfaces with the size of 4-20 nm and 50-100 nm after the cycles of photoreduction and thermal treatment was confirmed by SEM microscopy analysis of films (Fig. 9).

3.3 TiO_2 and TiO_2/ZnO films modified with Au nanopartiles produced by photo- and thermal treatment

The procedures of metal particles synthesis influence on the maximum position of SPR band of Au NPs (Fig.10). For the films obtained by thermo- and photo-thermo procedures, the gold particles are spherical whereas adsorption brings to the nanorods with low aspect ratio as it is indicated in (Rodrı´guez-Ferna´ndez et al, 2005; Eustis & El-Sayed, 2005; Eustis & El-Sayed, 2006). It must be noted that the more intensive and well-defined SPR maxima were registered for the films containing zinc ions indicating the higher dispersion of metal crystallization centers near zinc ions in titania matrix preventing the NP's aggregation in the clusters (Manujlov et al, 2008).

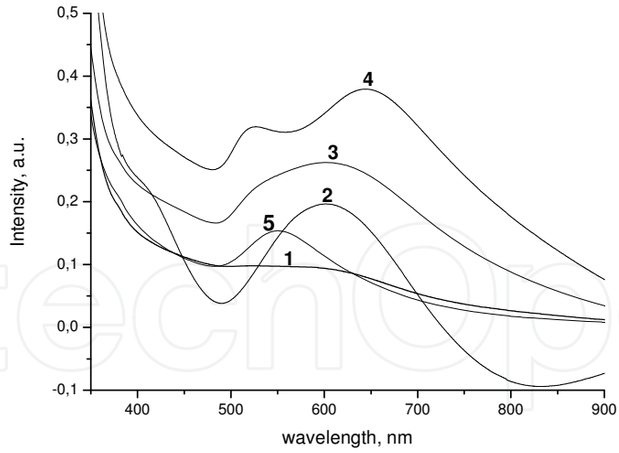

Fig. 10. Absorption spectra of gold-doped films: 1. TiO_2/Au_t; 2. $TiO_2/ZnO/Au_t$ (λ_{max}= 600 nm); 3. TiO_2/Au_{ads} (λ_{max}= 600 nm); 4. $TiO_2/ZnO/Au_{ads}$ (λ_{max}= 518 and 645 nm); 5. $TiO_2/ZnO/Au_{tph\text{-}t}$ (λ_{max}= 545 nm).

The elemental maps of Ti, O, and Zn showed the homogeneous distribution of titanium, zinc and oxygen on the surface of $TiO_2/ZnO/Au$ films (not shown here). SEM images and corresponding Au maps (Fig. 11) depict the different sizes and homogeneous distribution of gold particles with the size in the range of 25-180 nm (dominate 25-40 nm) for the $TiO_2/ZnO/Au_t$ and 1-35 nm (dominate 3-10 nm) for $TiO_2/ZnO/Au_{ph\text{-}t}$ films (the particle size distribution is not shown). The gold particles in $TiO_2/ZnO/Au_{ads}$ are 25-250 nm (the major fraction is 70-110).

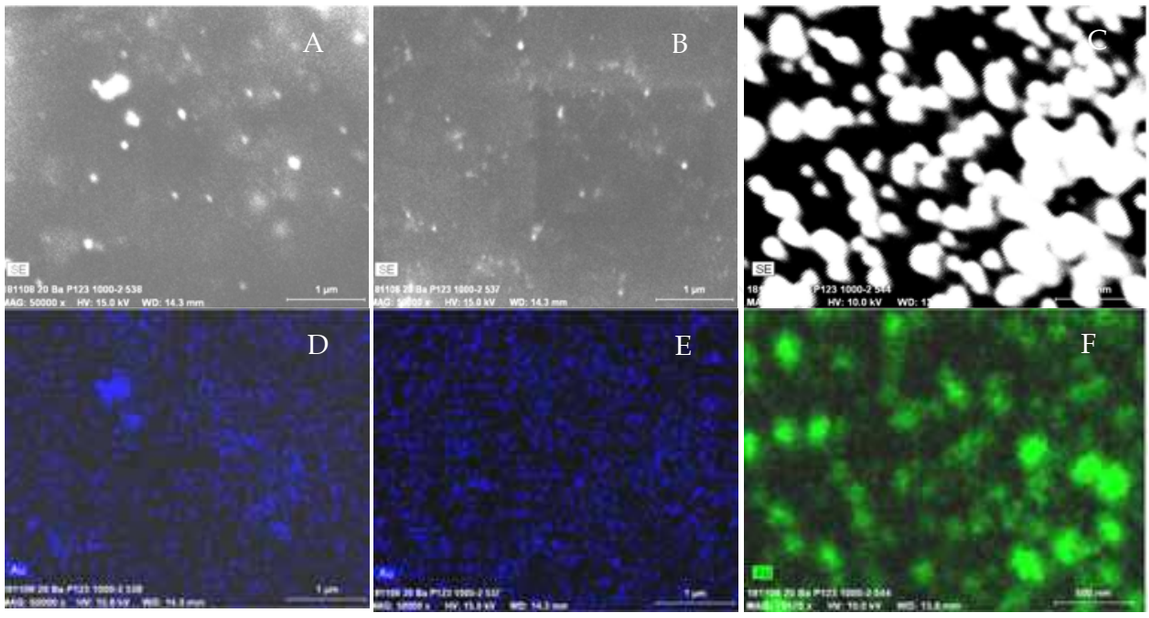

Fig. 11. SEM images and Au map of $TiO_2/ZnO/Au$ films: A, D- Au_t, B, E- $Au_{ph\text{-}t}$; C, F- Au_{ads}.

X-ray analyzed EDS spectra testify the zinc ions on the surface of the $TiO_2/ZnO/Au_t$ and $TiO_2/ZnO/Au_{ph\text{-}t}$ films contrary to Zn^{2+}/TiO_2 and $TiO_2/ZnO/Au_{ads}$ (not shown here). The enrichment of the film surface by zinc ions is suggested to be due to the formation of

complexes between zinc acetate and tetrachlorautic ions during sol ageing resulting in the localization of zinc ions near photoformed gold particles on the surface.

3.4 $TiO_2/ZrO_2/SiO_2$ films with embedded Ag and Au nanopartiles by thermal induced reduction

From the point of view of photocatalytic applications it was interesting to synthesize triple mixed oxides, which surface would have new active surface sites active in catalytic processes. In addition, modification of the last with metal nanoparticles could have positive influence on the charge separation in the semiconductor during its excitation by UV light. To fulfill these requirements we have synthesized by sol-gel method mixed $TiO_2/ZrO_2/SiO_2$ films modified with Ag and Au nanoparticles through thermal reduction of noble metal ions in the mixed matrix during its sintering.

No absorption characteristic for nanosized silver particles was detected in the absorbance spectra of $TiO_2/ZrO_2/SiO_2/Ag$ films with different percentage of silver after their sintering at 500°C. Similar picture was already described for TiO_2/Ag films with photodeposited silver particles after heat treatment at temperatures above 500°C. We believe that this means rather formation of the tiny silver particles on the surface of nanocomposite films with oxide shell than the absence of the nanosilver. SEM microscopy of surface of $21\%TiO_2/9\%ZrO_2/70\%SiO_2/Ag$ film (Fig. 12 a) proves the formation of flake-like particles in the subsurface/surface region of the film with the size of about 30 nm, most probably, corresponding to the silver particles covered with thick oxide shell. This will be further confirmed by the XPS investigations of the surface of the composites.

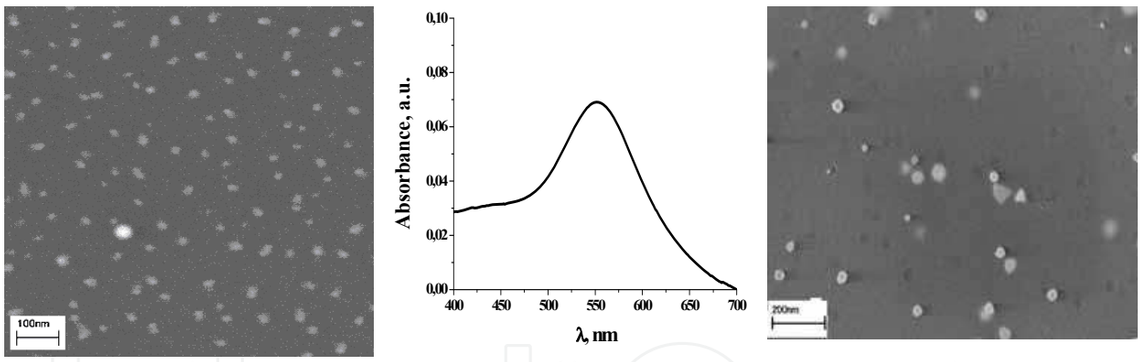

a) b) c)

Fig. 12. SEM images of surface (a, c) and absorbance spectrum (b) of $TiO_2/ZrO_2/SiO_2/Ag$ (5%) (a) and $TiO_2/ZrO_2/SiO_2/Au$(3,4%) (b, c) films after sintering at 500 ^{0}C.

In absorption spectrum of $TiO_2/ZrO_2/SiO_2/Au$ film (Fig. 12 b) the surface plasmon band of gold nanoparticles is observed at 550 nm. The surface of $TiO_2/ZrO_2/SiO_2/Au$ films is covered with gold nanoparticles of different shapes – triangular pyramids and spheres that can be seen from SEM image (Fig. 12 c). Big amount of voids on the films surface, with the shape corresponding to the one of metal nanoparticles formed, confirms heat induced movement of reduced metal clusters/nanoparticles as a result of their agglomeration and/or leaving of the surface into gas phase.

Optical absorption spectra of $TiO_2/ZrO_2/SiO_2/Au$ films with different content of gold introduced into the sol for films are presented in the Fig. 13. The position of SPR band shifts consistently to longer wavelengths region from 549 to 554 nm with increasing Au^{3+} concentration from 1 to 7 mol.% in the films. According to data available in the literature

(Epifani et al, 2000; Selvan et al, 1998; Sung-Suh et al, 2004) it means an increase of the size of Au nanoparticles after thermal treatment of the films.

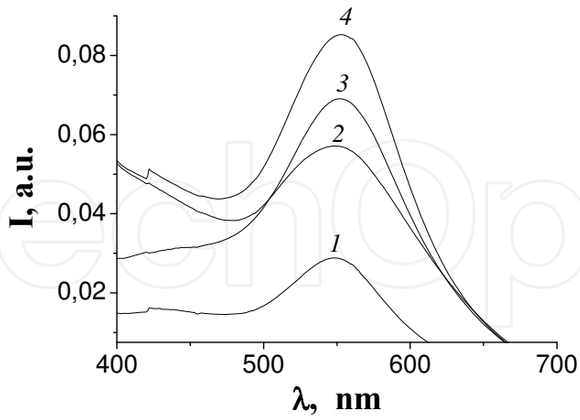

Fig. 13. Optical absorption spectra of $TiO_2/ZrO_2/SiO_2$ films with various percentages of gold: *1* – 1 % Au; *2* – 3,4 % Au; *3* – 5 % Au; *4* – 7 % Au.

In summary, synthesis strategy employed for the preparation of composite materials determines final localization of noble metal nanoparticles. Single step thermal reduction of noble metal ions during sintering of sol-gel films leads to the distribution of metal nanoparticles within the bulk of the films as well as partial localization of the particles on the films surface. Dual step modification of the films surface by photoreduction of silver ions and subsequent composites thermal treatment results in uniform modification of surface rather than bulk of the films by Ag nanoparticles with narrow particles sizes distribution. The last is being determined by the leaching of ZnO from the surface of composite films with subsequent localization of tiny Ag nanoparticles on these sites.
Photoreduction of tetrachloroauric ions in the "wet" films leads to the formation of the homogeneous distributed gold nanoparticles with the sizes to 10 nm where the subsequent thermal treatment did not cause to its aggregation. The mechanism of thermal reduction is differed from the former case that is the reason of enlargement of gold particles due to the easier diffusion of gold (I) ions formed on the first stage of thermal treatment (scheme). Photoreduction of adsorbed $AuCl_4^-$ ions on the Zn^{2+}/TiO_2 film surface creates rod-shaped nanosized gold particles.

4. XPS investigations

4.1 SiO_2/Ag and SiO_2/Au

Electronic structure of the composite films has been investigated by means of X-Ray photoelectron spectroscopy. The main contribution to the Ag3*d*-line of the SiO_2/Ag film and to the Au4f-line of the SiO_2/Au film have the components with the binding energy (E_B) $Ag3d_{5/2}$ = 370.84 eV (Fig. 14 a) and E_B $Au4f_{7/2}$ = 85.61 eV (Fig. 14 b), correspondingly. The position of these lines is slightly shifted towards higher energies comparing to the ones reported for the gold and silver foils [Kamat et al, 2002].
As we reported previously [Suzer/Jashan article], these shifts might be explained by the chemical interactions between metal nanoparticles and oxide matrix. By applying external voltage bias during XPS analysis of the SiO_2/Ag-Au sol-gel films linear parallel shift of the Si2p, Au4f, Ag3d and O1s signals was observed revealing chemical interaction between metal nanoparticles and silicon oxide matrix.

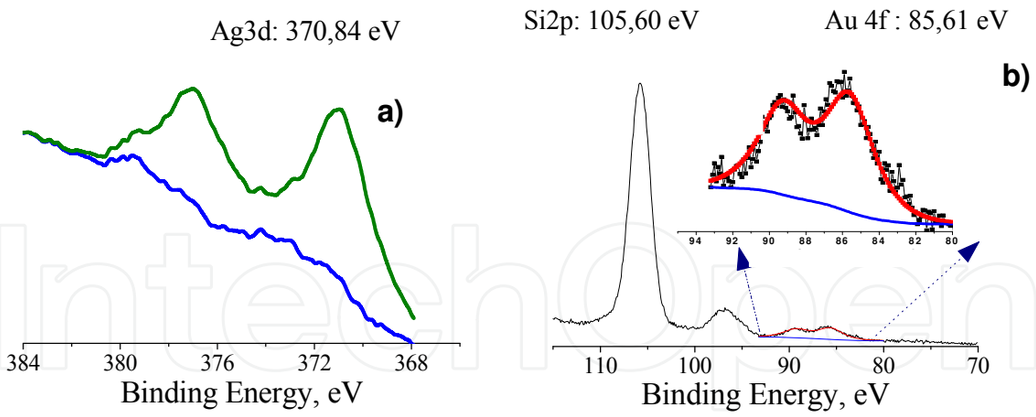

Fig. 14. XPS-spectra of Ag3d a) and Si2p and A4f b) –levels for SiO_2/Ag and SiO_2/Au mesoporous films.

4.2 TiO_2/Ag and TiO_2/ZnO/Ag films

In the XPS spectrum of the TiO_2 film with silver nanoparticles produced by thermal induced silver reduction (Fig. 15) we have observed that the Ag3*d*-line is formed by the contribution of three silver states with E_B Ag$3d5_{/2}$ = 367.7 eV (silver oxide), 368.4 eV (metallic silver) and at 368.8 eV (charge transfer state).

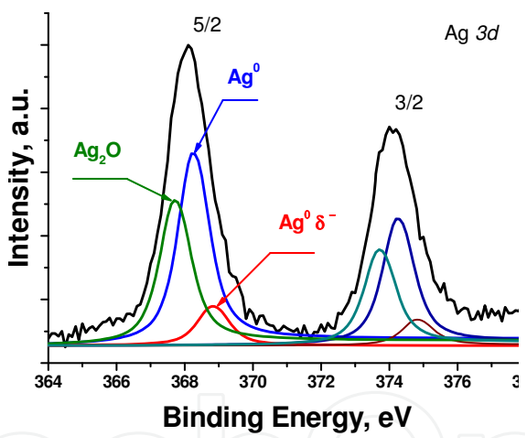

Fig. 15. XPS-spectra of Ag3d–levels for TiO_2/Ag film heat treated at 500°C.

Silver is a metal that has anomalous properties in E_B shifts when being oxidized, i.e. the Ag3*d* peaks shift to lower E_B values (Weaver & Hoflund, 1994). Usually, positive E_B shifts in the metal core-level peaks are observed when metal is oxidized that is explained by considering the electronegativity differences between metal atom and cation. Factors such as lattice potential, work function changes, and extra-atomic relaxation energy leads to negative E_B shift in the case of Ag and some Cd compounds (Xin et al, 2005).

Thus, it can be concluded that in the process of thermal reduction of silver ions while TiO_2 inorganic matrix formation we obtain silver nanoparticles embedded into inorganic matrix covered with silver oxide shell. On the other hand, when silver nanoparticles containing nanocomposites are prepared through photoreduction and subsequent thermal treatment, different states of silver, contributing to the Ag3*d*-line in the XPS spectra, have been observed in comparison to the samples described before.

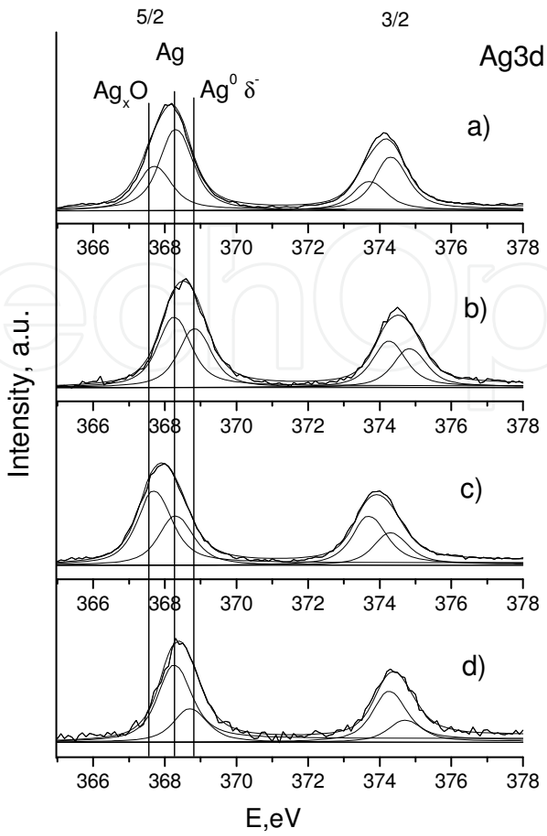

Fig. 16. XPS-spectra of Ag3d-levels for as-prepared samples with photoreduced silver particles (a, c), and after thermal treatment at 500°C (b, d) of TiO_2/Ag (a, b) and TiO_2/ZnO/Ag (c, d) films.

Ag3$d_{5/2}$ component for as-prepared TiO_2/Ag and TiO_2/ZnO/Ag films stands at 368.2 and 368.0 eV respectively (Fig. 16, a, c). Thermal treatment results in the peak narrowing and their shifts toward higher binding energy by 0.4eV. The peak decomposition reveals the presence of Ag in metallic state peaked at 368.35 eV and Ag_2O with peak at E_B = 367.7 eV. The values are in good agreement with those (368.22 eV) reported in (Krylova et al, 2006; Gregg & Sing, 1982). These results indicate that the silver nanoparticles formed on TiO_2 under given experimental conditions (UV irradiation, ambient atmosphere, room temperature) are chemically very reactive and were easily oxidized with Ag_2O shell formation. Authors (Nguyen, 1999) reported that the grows of silver oxide overlayer up to 6 nm on Ag° – TiO_2 interface is a function of plasma exposure time at room temperature. Higher intensity of oxide peak for TiO_2/ZnO/Ag film as compared to TiO_2/Ag supports our assumption about more homogeneous distribution of smaller Ag nanoparticles on this surface. Tendency to oxidation might be increased significantly with decrease of particle size and increase of portion of surface atoms exposed to interface.

Annealing at 500°C results in the complete decomposition of silver oxide, no peaks are observed at low E_B side near 367.7 eV for TiO_2/Ag as for TiO_2/ZnO/Ag samples (Fig. 16, b, d). For the last one Ag_2O decomposition leads to Ag° peak intensity growth (Fig 16, d) that coincides with narrow SPR band appearance in the absorption spectra (Fig 8 b).

For both samples two components were found to form Ag$3d_{5/2}$ peak: one of them at 368.4 eV corresponds to metallic silver and the other one that has binding energy higher by 0.4 eV (368.8 eV) than that for Ag^o. Observed shift towards higher E_B after thermal treatment is similar to reported for Ag nanoparticles in SiO_2, SiN_x and TiO_2 thin films (Gun`ko & Mikhalovsky, 2004). This effect was observed also for Pt (Crepaldi et al, 2003) indicating charge transfer from semiconductor matrix to the metal.

XPS data confirm our suggestion that Ag^o is still presented on the TiO_2/Ag film, but the disappearance of SPR band in the TiO_2/Ag spectra could be caused by the formation of very small Ag particles on the TiO_2 surface or by partial "dissolving" of certain critical size silver nanodrops in the crystalline matrix as it was described elsewhere (Shacham et al, 2004; Shter et al, 2007). Escape of the metal nanoparticles from TiO_2/1%ZnO/Ag film after 500°C treatment leads to the more homogeneous particle size distribution through the film profile because of more intensive evaporation of silver droplets from the outer surface of the films occurs. The smaller particles that manifested in the intensive SPR peak in the absorption spectra were formed in restricted media inside the film pores, where Zn^{2+} ions were replaced by Ag^+ one and converted to Ag^o as a result of photoreduction. Similar results are reported for temperature dependence of Ag nanoparticles distribution through the depth profile of Ag-TiO_2 sol-gel films (Crepaldi et al, 2003).

4.3 TiO_2/ZnO/Au films

Nonsymmetrical Ti (2p) peaks registered in the spectra of all samples were deconvoluted as the sum of 458.9 and 458.5 eV peaks corresponded to Ti-O-Ti and Ti-O-Zn bonds (not shown here). No XPS peak of Zn (2p) is obtained for $Au_{ads}/Zn^{2+}/TiO_2$. The peak attributed to the formation of Ti-O-Zn (E_{BE}=1022.5 eV) is predominated over the Zn-O-Zn one (E_{BE}=1021.7 eV) for TiO_2/ZnO/Au_t and TiO_2/ZnO/$Au_{ph\text{-}t}$ in comparison with TiO_2/ZnO (Fig. 16). The XPS results and X-ray analyzed EDS spectra clearly show that gold NP's are responsible for the acceleration of anatase crystallization and formation of $Zn_2Ti_3O_8$ phase detected by XRD analysis (Smirnova et all, 2010).

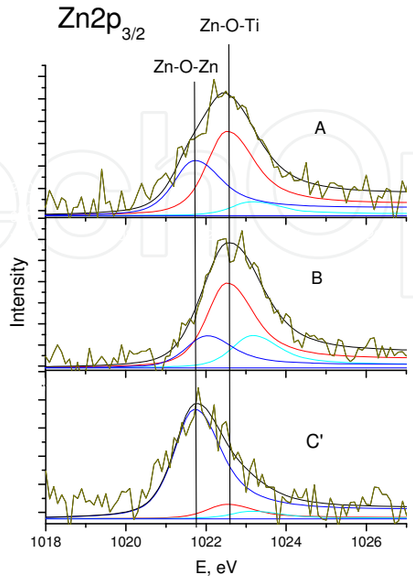

Fig. 17. XPS spectra of $Au_{ph\text{-}t}/Zn^{2+}/TiO_2$ (A), $Au_t/Zn^{2+}/TiO_2$ (B) and Zn^{2+}/TiO_2 (C').

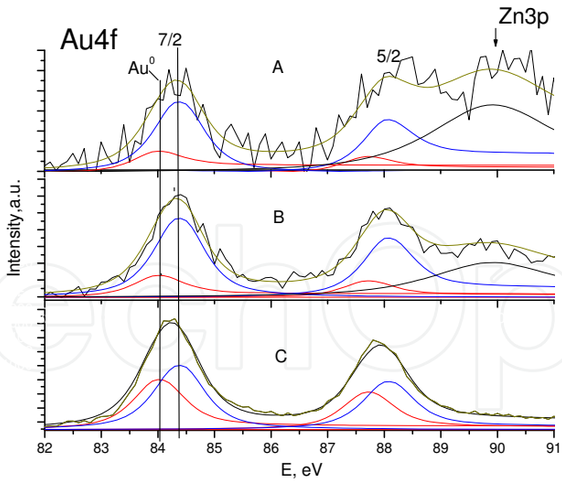

Fig. 18. XPS spectra of $Au_{ph\text{-}t}/Zn^{2+}/TiO_2$ (A), $Au_t/Zn^{2+}/TiO_2$ (B) and $Au_{ads}/Zn^{2+}/TiO_2$ (C).

Binding energy (BE) of Au $4f_{7/2}$ peaks (84.3 eV) is deconvoluted in doublet for the gold containing films. BE signals at 84.0 and 84.4 eV can be related to the bulk of metallic gold and gold clusters, respectively, as reported (Ozkaraoglu et all, 2007). The intensity of signal attributed to the clusters predominates the intensity of bulk gold for $TiO_2/ZnO/Au_{ph\text{-}t}$ and $TiO_2/ZnO/Au_t$ samples (Fig. 17 A and B) contrary to $TiO_2/ZnO/Au_{ads}$ (Fig. 18). It is concluded that the correlation between the gold sizes and contribution of Au clusters on the surface is achieved.

4.4 $TiO_2/ZrO_2/SiO_2$ films with embedded Ag and Au

The XPS spectra of silver and gold nanoparticles in ternary oxide films are presented in Fig. 19 and Fig. 20 respectively. In silver Ag 3d region the fitted spectra consist of two main peaks – Ag $3d_{5/2}$ and Ag $3d_{3/2}$ doublet. Ag $3d_{5/2}$ peak position at 367.99 eV (Fig. 18, thick line) is in good agreement with 368.196 eV reported in (Nirmalya et all, 2007), 368.22 eV in (Matsuoka et all, 1997) and 367.98 eV in (Zhang et all, 2000) for metallic silver.

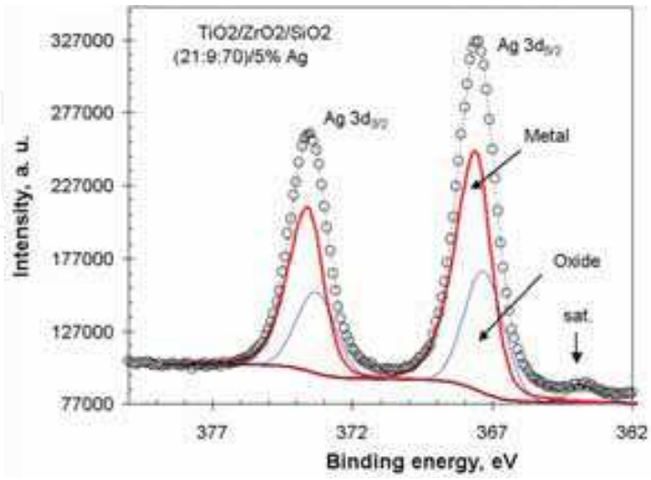

Fig. 19. Fitting procedure for Ag 3d spectra for mixed oxides film modified with silver nanoparticles $TiO_2/ZrO_2/SiO_2$ (21:9:70)/ 5%Ag: circles – experimental data, dashed line – fitted curve; thick line - metallic silver, thin line – silver oxide.

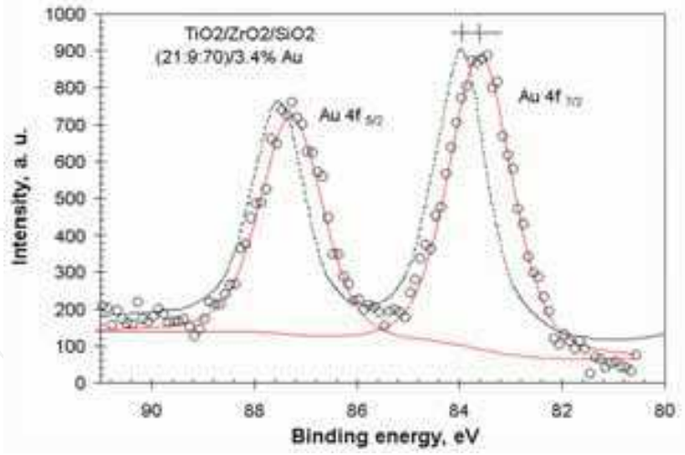

Fig. 20. Fitted Au 4f spectra of $TiO_2/ZrO_2/SiO_2$ (21:9:70)/3.4%Au film and gold reference spectra: circles – experimental data, thin lines – fitted curve; dashed line - literature data (Matsuoka et all, 1997).

Fitting procedure results for gold Au 4f region are presented in Fig. 20. In this figure the literature data reported in (Matsuoka et all, 1997) are compared with the experimental data. Peaks corresponding to gold oxide were not detected. Small shift of Au $4f_{7/2}$peak by 0.2 eV towards lower binding energy values was found.

Au 4f doublet peaks were detected by XPS at sufficient intensity, peaks position and shape (Fig. 20) coincide with literature data (Matsuoka et all, 1997) nevertheless considerable disagreement between Au molar and surface atomic concentrations was found (3,4 mol.% and 0,4 at.%). This disagreement can be related to the differences in Au concentration over the film profile.

Hence, XPS measurements confirm that gold and silver generated nanoparticles are mostly present in metallic state. The silver state in the composite films strongly depends on the chosen synthesis strategy. Oxide layer of silver nanoparticles is being destroyed by thermal treatment (500 °C) for the films prepared by photoreduction with further thermal treatment whereas for the films prepared through single step thermal reduction silver particles are covered by oxide shell. The growth of gold clusters fraction and Zn-O-Ti bond formation were registered in XPS spectra for the materials with smaller particle sizes prepared by photo- or thermoreduction.

5. Photocatalytic properties

Among studied oxide composite materials modified with metal nanoparticles titanium dioxide itself or its mixtures with other oxides: SiO_2, ZrO_2, ZnO demonstrate good photocatalytic properties under illumination with UV or visible light. As was already mentioned before, modification of photocatalysts with metal nanoparticles either embedded within the film or deposited onto their surface strongly increases photoactivity of the photoactive catalytic materials through the improvement of charge separation processes (Sclafani et al, 1997; Submanian, 2001).

Photocatalytic activity of the titania based materials studied in present investigation has been widely examined in different environmentally important processes.

5.1 TiO_2/Ag films

The photocatalytic activity of mesoporous TiO_2/Ag films with thermally reduced Ag nanoparticles was tested using the process of xantene dye Rhodamine B (RB) degradation in aqueous solutions. Under UV irradiation (λ = 254 nm) the absorption peaks corresponding to Rhodamine B diminished and finally disappeared, indicating degradation of the dye. No new absorption bands were observed, in contrast to Sung-Suh et al, 2004, where significant (-50 nm) shift of the long wave absorption band of Rhodamine B was reported indicating de-ethylation process. So we can suggest that Rhodamine B photooxidation in our experiments proceeds through the degradation of chromophore chains in the solution. To compare the photoactivity of TiO_2 and TiO_2/Ag films with Ag contents from 1 to 10 at.%, the rates of the dye photodegradation process were calculated from a pseudo first-order reaction rate approximation for equal reaction conditions (see Table 1).

Sample	UV light		Visible light	
	k, min^{-1}	$\tau_{0,5}$, h	k, min^{-1}	$\tau_{0,5}$, h
Blank experiment	1.6×10^{-3}	7.1	$2.5\cdot10^{-6}$	76.7
TiO_2	3.5×10^{-3}	3.3	$1.3\cdot10^{-5}$	15.3
TiO_2/Ag 1% (at.)	6.0×10^{-3}	1.9	-	-
TiO_2/Ag 3% (at .)	6.2×10^{-3}	1.9	$1.3\cdot10^{-5}$	14.7
TiO_2/Ag 5% (at.)	6.8×10^{-3}	1.7	$4.2\cdot10^{-5}$	4.6
TiO_2/Ag 10% (at.)	4.3×10^{-3}	2.7	$4.9\cdot10^{-5}$	3.9

Table 1. The rate constants of photodegradation of RB in the presence of TiO2/Ag films.

As it is showed in the table, a maximal efficiency (two times higher in comparison to pure TiO_2 film) was observed for TiO_2/Ag films with an Ag content of 5 at.%. Further increase of the dopant content leads to a decrease of TiO_2/Ag photocatalytic activity. According to Refs. 4. 5. and 13 (Manujlov et all, 2008) doping of the semiconductor with low concentrations of noble metal nanoparticles is advantageous to promote charge separation processes but with increasing metal concentrations the processes of hole trapping by negatively charged metal nanoparticles become predominant leading to depressing of photocatalysis.
In the case of visible light excitation of TiO_2/Ag with different silver nanoparticles content it was observed steady increase of the photocatalytic activity of films with increasing of silver nanoparticles loading in the samples (see Table). Obviously, this difference of the photocatalytic activity of the TiO_2/Ag film dependence on the silver nanoparticles content in the case of excitation with UV or visible light is related to the different mechanisms of the dye molecule degradation (Sung-Suh et al, 2004).

5.2 TiO_2/ZrO_2/SiO_2 films with embedded Ag and Au nanoparticles

Photocatalytic degradation of Rhodamine B dye in the presence of ternary TiO_2/ZrO_2/SiO_2 films modified with noble metal nanoparticles under UV-light irradiation proceeds according to the same scheme as for the TiO_2/Ag and ZnO/TiO_2/Ag films, i.e. without/with minor impact of de-ethylation procecess but mainly through the dye chromophore degradation steps. As it was expected, ternary oxide systems with embedded noble metal nanoparticles have higher photocatalytic activity than that for unmodified TiO_2/ZrO_2/SiO_2 films. The rate constants are presented in the Table 2.

Sample	Rate constants, k*10^{-3} min^{-1}
$TiO_2/ZrO_2/SiO_2$	1.4
$TiO_2/ZrO_2/SiO_2$/5 %Ag	2.0
$TiO_2/ZrO_2/SiO_2$/3,4 %Au	6.3

Table 2. The rate constants of photodegradation of RB in the presence of catalysts.

Comparing the photocatalytic activity of the films of ternary system, modified with gold and silver nanoparticles, it was found that in the presence of films containing silver, the rate constant of decomposition of the Rhodamine B is lower in comparison with Au modified films, when almost four-fold increase of photocatalytic activity in comparison with bare $TiO_2/ZrO_2/SiO_2$ film was observed. As the gold containing photocatalyst has the most promising photoactivity, Au nanoparticles concentration influence on the photocatalytic activity of $TiO_2/ZrO_2/SiO_2$ films was studied. We have found that there exists an optimum gold nanoparticles content (5 mol.%) in the ternary oxide system when the photocatalytic activity of the films increases by almost one order of magnitude comparing to the one for unmodified films. Further increasing of gold concentration cases deterioration of photocatalytic activity of the samples. The rate constants of the process of photocatalytic degradation of Rhodamine B dye in the presence of $TiO_2/ZrO_2/SiO_2$/Au films with different Au content are summarized in the Table 3.

$TiO_2/ZrO_2/SiO_2$/Au, mol.%	Rate constants, k*10^{-3} min^{-1}
1	6.0
3,4	6.3
5	10.2
7	5.3

Table 3. The rate constants of photodegradation of RB in the presence of $TiO_2/ZrO_2/SiO_2$/Au films with different gold content.

The observed dependence of the $TiO_2/ZrO_2/SiO_2$ films photocatalytic activity on the gold concentration has been attributed to the differences in size, quantity and homogeneous distribution of gold nanoparticles on the catalyst surface. As was proved by the AFM investigations of surface of $TiO_2/ZrO_2/SiO2$/Au films with different gold content (Vityuk et all, 2007), the surface coverage with gold nanoparticles continuously increases with increasing gold concentration in the films. Most probably, on the surface of the $TiO_2/ZrO_2/SiO_2$/Au films with low surface coverage with gold nanoparticles (1 and 3.4 mol.%), the recombination processes are more efficient than that in the films containing 5 mol.% of gold. Further increase in concentration of gold (more than 5 mol.%) is accompanied with aggregation of nanoparticles, which in turn leads to a screening of surface from irradiation and prevents direct contact of dye molecules with the surface of catalyst.

5.3 Photocatalytic activity of Ag (Au) ZnO/TiO_2 coatings in tetracycline hydrochloride (TC) degradation

The biological active compounds as antibiotics, hormones, preservatives and anesthetics have been identified in the aquatic environment and soil as the result of the extensive development of pharmaceutical industry and the wide consumption by human. Antibiotics are widely used against microbial infection in medicine and veterinary as well as the feed additives increasing the growth and prevent pathogens in animal farms and fisheries raising

the concerns over proliferation of antibiotic-resistant bacteria. Tetracycline is one of the most frequently prescribed groups of antibiotics. Residues of TC and their metabolites were detected in eggs, meat and animals based on different exposure methods (Ruyck et all, 1999; Zurhelle et all, 2000). Their accumulation in human organism can produce arthropathy, nephropathy, central nervous system alterations, spermatogenesis anomalies, possible mutagenesis and photosensitivity in human beings. Due to their antibacterial nature, antibiotic contaminated waters cannot be effectively eliminated by traditional biological methods (Kummerer et all, 2000). Tetracycline presents a class of the compound that is sensitive to light and classified as a phototoxic drug. Thus, TC residues in culture pond and on the surface of soil follow through the formation of the TC derivatives that could be even more dangerous for public health.

Destruction of the chemical bonds of the complex organic structure such as antibiotics tetracycline (Fig. 21) signified the unpredicted type of the products and thus the effect of reaction conditions on the reaction mechanism. TC molecule can behave as a cation, a neutral/zwitterion, an anion or a dianion depending on pH of the systems. Ring A absorbs only in the 250-300 nm area, whereas the BCD ring chromophore contributes to both 250-300 and 325-400 nm absorption bands as described in (Schneider et all, 2003).

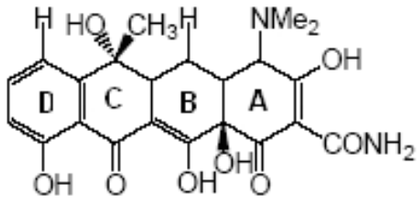

Fig. 21. The structural formula of TC.

Tetracycline presents a class of the compound that is sensitive to light and classified as a phototoxic drug. The photodecomposition products of TC, such as dedimethylaminotetracycline, anhydrotetracycline, lumitetracycline, oxytetracycline, quinone form, and fourteen others were detected at different reaction conditions (Davis et all, 1979; Moore et all, 1983; Sanniez et all, 1980). Furthermore, it is identified seven products of the TC photolysis under conditions similar to the natural ones (Oka et all, 1989).

The preliminary estimation of the photocatalytic efficiency can be performed by detailed monitoring of the TC absorption spectra during irradiation. The shifts of the maxima at 275 and 357 nm and the appearance of absorption at 400-500 nm are attributed to the formation of tetracycline derivates (Paola et all, 2004).

However, the steady and simultaneous fall of these two maxima without absorption in visible are registered at $TiO_2/ZnO/Au_t$ and $TiO_2/ZnO/Au_{ph\text{-}t}$ films leading to the suggestion of tetracycline degradation rather then oxidation. (Linnik et all, 2009). As seen from Fig. 22, irradiating the tetracycline at $Ag_t/ZnO/TiO_2$ brings to the less effective degradation than at $Au_t/ZnO/TiO_2$. In the presence of $TiO_2/ZnO/Ag$ films synthesized either thermo or adsorption methods, the TC transformation accompanied by the formation of oxidized products. Antibiotics adsorption on $TiO_2/ZnO/Au_{ph\text{-}t}$ film is reached to 58 % contrary to the adsorption inability of $TiO_2/ZnO/Au_{ads}$ and $TiO_2/ZnO/Au_t$ films. Comparing the absorption spectra of the film before the contact and after adsorption of TC the new absorption band at 420 nm is appeared (Fig. 23 A). Irradiation for 90 min brings to the gradual intensity decrease in the absorption spectra of the film as well as TC solution. Hence, the TC degradation takes place on the surface of $TiO_2/ZnO/Au_{ph\text{-}t}$ film through the adsorption-desorption equilibrium.

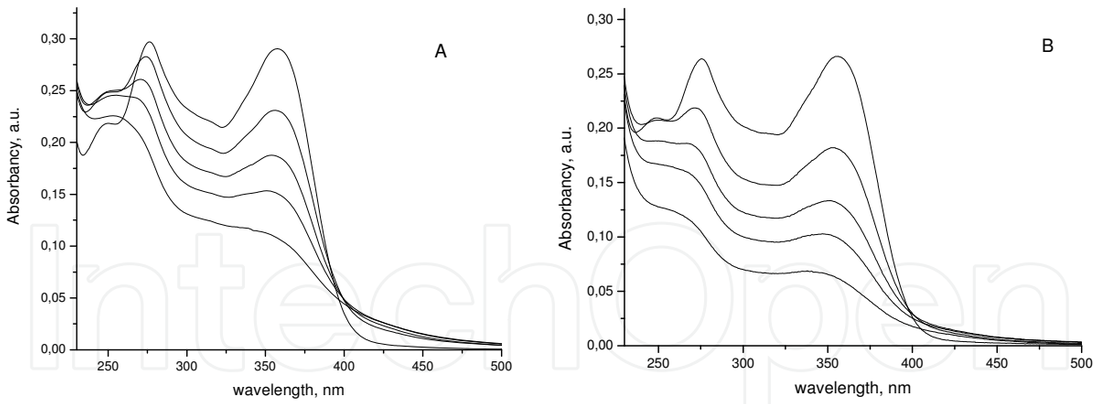

Fig. 22. Evolution of absorption spectra of tetracycline solution over TiO2/ZnO/Agt (A) and TiO_2/ZnO/Au_t (B) during 90 min irradiation.

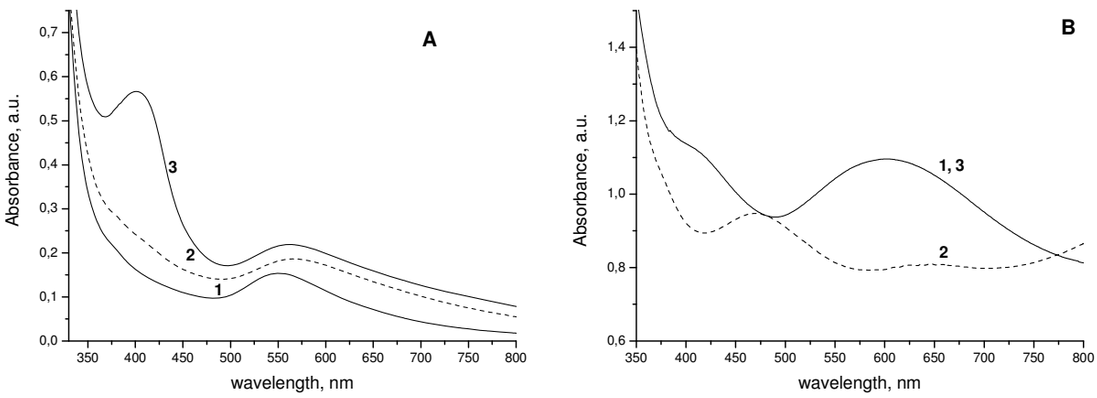

Fig. 23. Absorption spectra of $Au_{ph\text{-}t}$/ZnO/TiO_2 (A) and Au_t/ZnO/TiO_2 (B) films: 1-before contact; 2-after 90 min of irradiation; 3- after adsorption in the dark.

The shift of SPR band after 90 min irradiation in TC solution is observed in the absorption spectrum of the TiO_2/ZnO/Au_t film (Fig. 23 B). The initial view of the spectrum is achieved by keeping of the film in the dark and air with for 24 hours. The blue shift of SPR is supposed to be due to the oxidation of gold by the hole and/or hydroxyl radical and/or other radical generated during photocatalytic degradation of TC molecules accompanying the depletion of gold metal particles. The formed gold ions might be incorporated on the interface of Au particle and TiO_2. In the dark, the catalytic reduction of these ions by metal gold could followed as describe in (Gachard et all, 1998).

Photolysis of TC molecules (FW=444) resulted in the formation of anhydrotetracycline (FW=428), 4-epi-anhydrotetracycline (FW=426), oxytetracycline (FW=460), lumitetracycline (FW=399), dedimethylamino TC (FW=400), quinoid TC (FW=416) as the main products. The surface of the films is monitored using matrix free Laser desorption/ionization mass spectrometry (LDI) with the experimental parameters registered in the same manner as the liquid phases. The $Au_{ph\text{-}t}$/ZnO/TiO_2 and Au_t/ZnO/TiO_2 films as well as the solutions of TC before and during 90 min irradiation were compare for the level of TC degradation by MALDI measurements. Formation of aforesaid products is observed neither in the liquid phase nor on the film (Linnik et all, 2009). It is shown that the destruction of TC molecules

after 90 min irradiation is more efficient on the surface of $TiO_2/ZnO/Au_{ph\text{-}t}$ resulting in the appearance of the adsorbed product molecules with the less m/z values. The desorbed ion yield fragments of TC intermediates from the surface of $TiO_2/ZnO/Au_{ph\text{-}t}$ film after 20, 60, and 90 min irradiation are depicted in the scheme. TC molecule is adsorbed by amide group of ring A that leads to its destruction after 20 min irradiation. The adsorbed cyclic compounds are still present on the surface of the film after 60 min irradiation. Two main desorbed ion yield fragments (the highest percent values) show the mineralization of TC molecule.

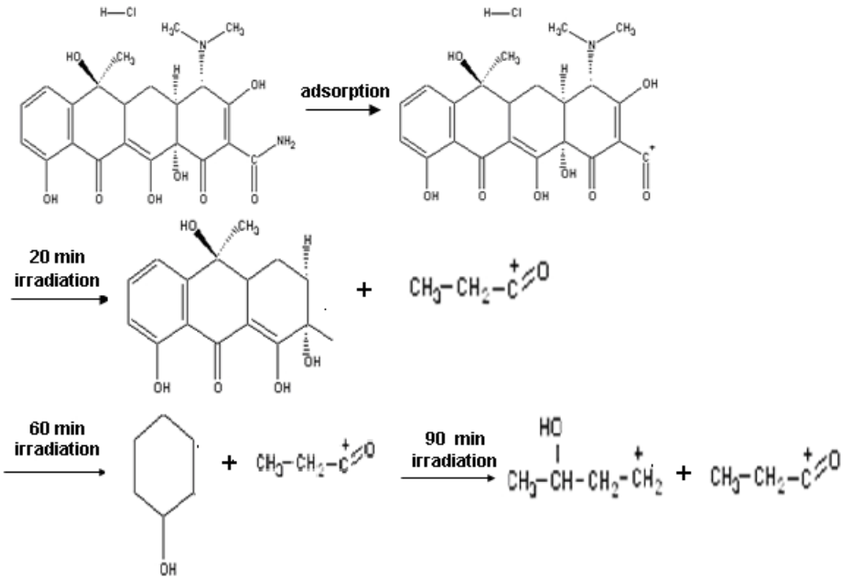

Scheme of the intermediates formation during the photocatalytic destruction of TC at $TiO_2/ZnO/Au_{ph\text{-}t}$ film.

Thus, the efficiency of photocatalytic TC destruction is affected by the size of gold nanoparticles where the mineralization of TC molecule is achieved on the surface of $TiO_2/ZnO/Au_{ph\text{-}t}$ film. Contrary to the gold-containing films, the oxidation of TC is observed over $TiO_2/ZnO/Ag$ composites.

6. Bactericide properties of stabilized silver and gold nanostructures on the surface of disperse silica

The nanoparticles of Ag and Au are used for the delivery of drugs (Jain, 2005; Paciotti et all, 2004; West & Halas, 2003), the treatment of wounds, the decontamination of water, and as bactericidal agents (Baker et all, 2005; Elchiguuerra et all, 2005; Pal et all, 2007; Shrivastava et all, 2007; Weir et all, 2008). Many bacteria are resistant to antibiotics, and it is therefore necessary to look for new bactericidal materials. Silver nanoparticles have a broad spectrum of antibacterial activity and are nontoxic for humans at low concentrations (Jin & Zhao, 2009). In large amounts, however, their toxicity is high, and the biocompatibility is substantially lower than for gold nanoparticles (Browning et all, 2009; Huang et all, 2008; Nallathambly et all, 2008; Song et all, 2010). The effectiveness of the nanoparticles can be intensified by depositing them on a support with a highly developed surface. In this respect

highly dispersed silica (HDS) is an ideal material. An important problem in the synthesis of nanoparticles is prevention or retardation of their aggregation and also oxidation at the stage of formation of the silver nanoclusters. In contrast to their state in the films, on the surface of dispersed silica the silver nanoparticles are unstable.

Therefore, in view of the diversity of potential applications of dispersed silica containing Ag nanoparticles on the surface, particularly as bactericidal agents, the stabilization of the nanoparticles of silver and their protection against oxidation and the influence of the surroundings represent an urgent task from the theoretical and applied view point. The principle of the stabilization of Ag nanoparticles with polymers or surfactants was applied successfully to the synthesis of composite systems based on highly dispersed silica (HDS) containing stable nanoparticles of silver with PVP and/or SDS as stabilizers (Mukha et all, 2009, 2010).

Samples of Ag/SiO_2 were synthesized by the adsorption of previously prepared colloidal solutions of nanosized silver

on the surface of dispersed silica. Nanosized silver in colloidal solution was obtained by chemical reduction from silver nitrate in the presence of sodium tetrahydroborate and a binary stabilizer – SDS and PVP. The obtained silver colloids were adsorbed on the surface of HDS. The concentration of Ag on the HDS amounted to 0.05%. The use of a binary stabilizer raises the stability of the silver nanoparticles. The interaction of the SDS and PVP consists of a combination of two processes: the formation of a complex as a result of hydrophobic interaction between the hydrocarbon unit of the SDS and the methylene groups of the PVP and electrostatic interaction between the head groups of the SDS and the partial charges of the nitrogen and oxygen of the pyrrolidol ring].

To explain the inhibitor effects of silver on bacteria it was suggested that silver reacted with proteins by combining the thiol (-SH) groups, leading to the bacteria inactivation (Traversa et all, 2001). In this work we examined the antibacterial activity of Ag/SiO_2 and Au/SiO_2 suspensions and Ag (Au) colloids. Ag/SiO_2 powders were tested after treating at 85-90°C, Au/SiO_2 – after 500°C. The probes have been diluted in distilled water with the concentration of 0,0016% wt. of metal NPs and 3,13 % wt. of HDS in suspension. Colloids were tested with the concentration of 0,0016 % wt. of metal NPs.

$AgNO_3$ solution has been used in the control experiments in the equal concentration as Ag NPs. Binary stabilizer PVP/SDS and $NaBH_4$ have been studied in the control with the same amount as in the colloids. Initial HDS has been tested also at the concentration 3,13% wt. in presence of the stabilizers and $NaBH_4$.

The results of antimicrobial activity of metal NPs in colloids and suspensions against E.coli, S.aureus и C.albicans are presented in the Table 4.

Essential reduction value for bacteria E.coli (5 lg) and fungi C.albicans (4 lg) in colloids achieved after 1 hour of exposure of microbial cells with Ag NPs. Staphylococcus were more Ag NPs-resistant, particularly 4,35 lg reduction achieved only after 4 hour. Decrease of Ag concentration allowed revealing mentioned phenomenon. C.albicans bacteria were the most sensitive among of studied objects.

The control $AgNO_3$ solution didn't show antimicrobial action. The same result also was revealed for PVP/SDS and $NaBH_4$ mixture. Thus presented experimental data indicate a high antimicrobial activity of silver colloids to all microorganisms.

Embedding of Ag NPs on SiO_2 surface slightly decrease activity of Ag/SiO_2 suspension. The exposure time increases and changes in interaction character of Ag NPs with the microbial cells appear. The contact time for 4 lg reduction achievement for C.albicans remained the

same as in colloid (1 h). At the same time Ag/SiO_2-resistance of E.coli rised. The reduction value was only 3,58 lg after 4 hour contact time. On the contrary, S.aureus was more sensitive then in colloid. But generally antimicrobial activity of Ag NPs/SiO_2 complex remained high. The nanosized gold at the same concentration range doesn't show antibacterial action on indicated microorganisms.

Samples and concentrations	Exposure time, h	test-strains, lgR*		
		E. coli	*S. aureus*	*C. albicans*
Ag NPs (0.0016 % wt) colloid	1	> 5.22	< 1.57	> 4.27
	2	> 5.22	2.07	> 4.27
	4	> 5.22	4.35	> 4.27
	24	> 5.22	> 5.24	> 4.27
initial microorganisms amount, lgN_0		7.37	7.39	6.42
Ag NPs (0.0016 % wt)/SiO2 (3.13 % wt)	1	< 1.39	3.89	> 4.54
	2	1.48	5.14	> 4.54
	4	3.58	> 5.17	> 4.54
	24	> 5.06	> 5.17	> 4.54
SiO2 (3.13 % wt) (control)	1	< 1.39	< 1.5	< 0.87
	2	< 1.39	< 1.5	< 0.87
	4	< 1.39	< 1.5	< 0.87
	24	< 1.39	< 1.5	< 0.87
initial microorganisms amount, lgN_0		7.21	7.32	6.69

Table 4. The antimicrobial activity of Ag NPs in colloids and suspensions.

7. Summary

In summary, synthesis strategy employed for the preparation of composite materials determines final localization of noble metal nanoparticles. Single step thermal reduction of noble metal ions during sintering of sol-gel films leads to the distribution of metal nanoparticles within the bulk of the films as well as partial localization of the particles on the films surface. In addition, intensive plasmon resonance absorption of metal nanoparticles can be obtained. Dual step modification of the films surface by photoreduction of silver ions and subsequent composites thermal treatment results in uniform modification of surface rather than bulk of the films by Ag nanoparticles with narrow particles sizes distribution. The last is being determined by the leaching of ZnO from the surface of composite films with subsequent localization of tiny Ag nanoparticles on these sites.

Such nanocomposites modified with metal nanoparticles are beneficial toward improving the efficiency of the photocatalytic oxidation – mineralization processes.

Photoreduction of tetrachloroauric ions in the "wet" films leads to the formation of the homogeneous distributed gold nanoparticles with the sizes to 10 nm where the subsequent thermal treatment did not cause to its aggregation. The mechanism of thermal reduction is differs from the former case that is the reason of enlargement of gold particles due to the easier diffusion of gold (I) ions formed on the first stage of thermal treatment.

The efficiency of photocatalytic Tetracycline destruction is affected by the size of gold nanoparticles where the mineralization of TC molecule is achieved on the surface of $TiO_2/ZnO/Au_{ph\text{-}t}$ film. Contrary to the gold-containing films, the oxidation of TC is observed over $TiO_2/ZnO/Ag$ composites.

The fixation of the metal nanoclusters on silica surface occurs due to a) interaction between the functional groups of stabilizer shell of NPs and OH-groups of silica and b) location of Me NPs within secondary pores of HDS globules. Obtained composite systems containing strongly bounded and homogeneously distributed on silica surface Ag NPs serve as potential wide-spectrum antimicrobial materials for medical and pharmaceutical application.

Thus, using photo-thermoreduction of appropriate ions within sol-gel oxide semiconductor/dielectric/metal composite films indicate simple and convenient way to produce improved photocatalysts sensitive to the visible, self-cleaning coatings, effective antimicrobial medium etc.

8. Acknowledgment

A. E., N. P. and Yu. M. thank the Governmental Target Scientific and Technical Center of Ukraine for financial support of part 6 of this work (Project N 5.16.1.7)

9. References

Alberius, P., Frindell, K., Hayward, R., Kramer, E., Stucky, G., Chmelka, B. (2002). General predictive synthesis of cubic, hexagonal and lamellar silica and titania mesostructured thin films. *J. Chem. Mater.*, Vol. 14, pp. 3284 – 3294.

Antonelli, D.M., Ying, J.Y. (1995). Synthesis of hexagonally packed mesoporous TiO_2 by modified sol-gel method. *Angew. Chem., Int. Ed. Engl.*, Vol. 34, pp. 2014 – 2017.

Arabatis, I.M., Stergiopolulos, T., Bernard, M.C. et al. (2003). Silver-modified titanium dioxide films for efficient photodegradation of methylorange. *Appl Catal B,* Vol.42, pp.187-201.

Baker, C., Pradhan, A., Pakstis, L., Pochan, D.J., Shah, S.I. (2005). Synthesis and antibacterial properties of silver nanoparticles. *J. Nanosci. Nanotechnol.*, Vol.5, pp.244-249.

Browning, L., Lee, K., Huang, T. (2009) Random walk of single gold nanoparticles in zebrafish embryos leading to stochastic toxic effects on embryonic developments. Nanoscale, Vol.1, pp.138-152.

Chaki, N.K., Tsunoyama, H., Negishi, U., Sakurai, H., Tsukuda T. (2007). Effect of Ag-Doping on the Catalytic Activity of Polymer-Stabilized Au Clusters in Aerobic Oxidation of Alcohol. *J. Phys. Chem. C.*, Vol.111, No.13, pp.4885 – 4888.

Chan, Y., Zimmer, J.P., Stroh, M., Steckel, J.S., Jain, R.K., Bawendi, M.G. (2004). Incorporation of Luminescent Nanocrystals into Monodisperse Core–Shell Silica Microspheres. *Adv. Mater.* Vol. 23-24, pp.2092-2097.

Crepaldi, E.L., Soler-Illia, G.J., Grosso, D., Cagnol, F., Ribot, F., Sanchez, C. (2003). Controlled Formation of Highly Organized Mesoporous Titania Thin Films: From Mesostructured Hybrids to Mesoporous Nanoanatase TiO_2. *J. Am. Chem. Soc.*, Vol. 125, pp.9770-9786.

Elchiguuerra, L.J., Burt, L.J., Morones, R.J., Camacho-Bragado, A., Gao, X., Lara H. H., Yacaman, M.J. (2005). Interaction of silver nanoparticles with HIV-1. *J. Nanobiotechnol*., Vol. 3, pp.1-10.

Epifani, M., Giannini, C., Tapfer, L., Vasanelli, L. (2000). Sol-gel synthesis and characterization of Ag and Au nanoparticles in SiO_2, TiO_2, and ZrO_2 thin films. *J. American Ceram. Society*., Vol. 83, No.10, pp. 2385 – 2393.

Eustis, S. & El-Sayed, M. A. (2005). The Aspect Ratio Dependence of the Enhanced Fluorescence Intensity of Gold Nanorods: Experimental and Simulation Study. *J. Phys. Chem. B*, Vol.109, No.34, pp.16350-16356.

Eustis, S. & El-Sayed, M. A., (2006). Determination of the Aspect Ratio Statistical Distribution of Gold Nanorods in Solution from a Theoretical Fit of the Observed Inhomogeneously Broadened Longitudinal Plasmon Resonance Absorption Spectrum. *J. Appl. Phys*, Vol. 100, No. 4, Article ID 044324.

Gachard, E., Remita, H., Khatouri, J., Keita, B., Nadjo, L., Belloni, J. (1998). Radiation-induced and chemical formation of gold clusters. *New J. Chem*., Vol. 22, pp.1257-1265.

Gnatiuk, Yu., Smirnova, N., Eremenko, A., Oranska, O., Chuiko, O. (2005). New nanostructured mesoporous film materials based on ZrO_2/TiO_2 for photooxidized destruction of 2,4- dinitroanilin. *Reports of NAS of Ukraine,* Vol. 8, pp. 143 – 148.

Gnatyuk, Yu., Manuilov, E., Smirnova, N. et al. (2006). Sol-gel produced mesoporous Ag/TiO_2 coatings effective in rhodamine B photooxidation. *Springer*, In: Kassing R et al (ed) NATO Science Series. II. Mathematics, Physics and Chemistry. Functional properties of Nanostructured Materials. Vol.223, pp.485-490. TheNetherlands.

Gnatyuk, Yu., Smirnova, N., Eremenko, A. et al. (2005). Design and photocatalytic activity of mesoporous TiO_2/ZrO_2 thin films. *Ads Sci & Technol*. Vol.23, pp.497–508.

Gonella, F., Mattei, G., Mazzoldi, P., Battaglin, G., Quaranta, A., De, G., Montecchi, M. (1999).Structural and optical properties of silver-doped zirconia and mixed zirconia-silica matrices obtained by sol-gel processing. *J.Chem. Mater*., Vol. 11, pp. 814 – 821.

Gregg, S.J. & Sing, K.S. (1982). *Adsorption, surface area and porosity*, second ed. Academic Press,.ISBN 0123009561, London.

Gun'ko, V.M. & Mikhalovsky, S.V. (2004). Evaluation of slitlike porosity of carbon adsorbents. Carbon, Vol.42, pp. 843- 849.

He, C., Yu, Y., Hu, X., Larbot, A. (2002). Influence of silver doping on photocatalytic activity of titania films. *Appl. Surf.Sci.,* Vol. 200, pp. 239-247.

He, J., Ichinose, I., Kunitake, T., Nakao, A. (2003). In situ synthesis of noble metal nanoparticles in ultrathin TiO_2-gel films by combination of ion-exchange and reduction processes. *Langmuir*, Vol. 18, pp.10005-100010.

Hirakawa, T., Kamat, P.V. (2004). Electron Storage and Surface Plasmon Modulation in $Ag@TiO_2$ Clusters. *Langmuir*, Vol. 20, pp.5645-5647.

Huang, T., Nallathamby, P. & Xu, X. (2008). Photostable single-molecule nanoparticle optical biosensors for real-time sensing of single cytokine molecules and their binding reactions. *J. Am. Chem. Soc.*, Vol.130, pp.17095-17105.

Huang, W., Qian, W. & El-Sayed, M. (2004). Coherent Vibrational Oscillation in Gold Prismatic Monolayer Periodic Nanoparticle Arrays. *Nano Letters*, Vol. 4, pp. 1741-1747.

Huang, X., El-Sayed, I. H., Qian, W., El-Sayed, M. A. (2006). Cancer Cell Imaging and Photothermal Therapy in the Near-Infrared Region by Using Gold Nanorods. *J. Am. Chem. Soc.*, Vol.128, pp.2115-2120.

Jain K. K. (2005). Nanotechnology-based drug delivery for cancer. *Technol. Cancer Res. Treat.*, Vol. 4, pp. 407-416.

Jain, P. K., Lee, K. S., El-Sayed, I. H., El-Sayed, M. A. (2006). Calculated absorption and scattering properties of gold nanoparticles of different size, shape, and composition: applications in biological imaging and biomedicine, *J.Phys. Chem. B*, Vol.110, No. 14, pp.7238-7248.

Jin, Y., Zhao, X. (2009). Cytotoxicity of Photoactive Nanoparticles, in Safety of Nanoparticles. *Springer*, edited by Tomas J. Webster, pp.19-31, ISBN978-0-387-78607-0, New York, USA.

Kamat, P. (2003). Influence of Metal/Metal Ion Concentration on the Photocatalytic Activity of TiO_2-Au Composite Nanoparticles. *Langmuir,* Vol.19*,* pp.469-474 469.

Kamat, P. V. (1993). Photochemistry on Nonreactive and Reactive (Semiconductor) Surfaces. *J.Chem. Rev*., Vol. 93, pp. 207 – 300.

Kamat, P.V. (1997). Composite Semiconductor nanoclusters. In: Kamat PV, Meisel D (ed) Elsevier Science. Semiconductor Nanoclusters – Physical, Chemical and Catalytic Aspects. Amsterdam

Kamat, P.V., Flumiani, M., Dawson, A. (2002). Metal-metal and metal-semiconductor composite nanoclusters. *Coll. Surf. A: Physicochem. Eng. Aspects*, Vol. 202, pp.269-279.

Kelly, K. L., Coronado,E., Zhao, L.L., Schatz, G.C. (2003). The Optical Properties of Metal Nanoparticles:

Kim, J., Song, K.C., Foncillas, S., Pratsinis, S.E. (2001). Dopants for synthesis of stable bimodally porouse titania. *J. Europ. Ceram. Society*, Vol. 21, pp. 2863 – 2872.

Kreibig, U., Vollmer, M. (1995). Optical properties of metal clusters*, Springer*, ISBN10 0387578366, 3540578366, Berlin.

Krylova, G.V., Gnatyuk, Yu.I., Smirnova, N.P., Eremenko, A.M., Gunko, V.M. (2009). Ag nanoparticles deposited onto silica, nitania and zirconia mesoporous films synthesized by sol-gel template method. *J. Sol-Gel Sci. Technol*, Vol. 5, No.2, pp. 216-228.

Kummerer, K., Al-Ahmed, A., Mersch-Sundermann, V. (2000). Biodegradation of some antibiotics, elimination of the genotoxicity and affection of wastewater bacteria in a simple test. *Chemosphere*, Vol.40, pp.701-710.

Lance, K.K., Coronado, E., Zhao, L., Schatz, G.C. (2003). The optical properties of metal nanoparticles; the influence of size, shape and dielectric environment. *J. Phys. Chem. B,* Vol. 107, pp. 668-677.

Liao, S., Donggen, Y., Yu, D. et al. (2004). Preparation and characterisation of ZnO/TiO_2, $SO_4^{2-}/ZnO/TiO_2$ photocatalyst and their photocatalysis. *J Photochem Photobiol A,* Vol.168, pp.7–13.

Link, S. & El-Sayed, M. A. (2001). Spectroscopic determination of the melting energy of a gold nanorod. *J Chem. Phys,* Vol.114, pp. 2362-2369.

Linnik, O., Manuilov, E., Snegir, S., Smirnova, N., Eremenko, A. (2009). Photocatalytic degradation of tetracycline hydrochloride in aqueous solution at ambient conditions stimulated by the gold containing zinc-titanium oxide films. *J. Adv. Oxid. Technol.*, Vol.2, No.12, pp.551-560.

Liz-Marzan, L.M., Giersig, M., Mulvaney, P. (1996). Synthesis of Nanosized Gold−Silica Core−Shell Particles. Langmuir, Vol.12, pp. 4329-4335, doi: 10.1021/la 9601871.

Lopez, T., Gomez, R., Sanchez, E., Tzompantzi, F. (2001). Photocatalytic ativity in the 2,4-Dinitroaniline decomposition over TiO_2 sol-gel derived catalysts. J. *Sol-Gel Science and Technol.*, Vol. 22, pp. 99 – 107.

Manujlov, E., Gnatyuk, Yu., Smirnova, N., Eremenko, A., Vorobets, V., Kolbasov, G., Guobiene, A., Tamulevicius, S. (2008). Mesoporous TiO_2 and TiO_2/ZnO/Ag films: sol-gel synthesis, photoelectrochemical and photocatalytic properties. *NATO Science for Peace and Security Series C: Environmental Security*, "Sol-Gel Methods for Materials Processing. Focusing on Materials for Pollution Control, Water Purification, and Soil Remediation". (Eds: P. Innocenzi, Yu.Zub and V. Kessler), pp. 427-434.

Marci, G., Augugliano, V., López-Muñoz, M.J. et al. (2001). Preparation, characterization and photocatalytic activity of polycrystalline ZnO/TiO_2 systems. I. Surface and bulk characterization. *J Phys Chem B*, Vol.105, pp.1026-1040.

Matsuoka, J., Naruse, R., Nasu, H., Kamiya, K. (1997). Preparation of gold microcrystal-doped oxide optical coatings through adsorption of tetrachloroaurate ions on gel films. *J. of Non-cryst. sol.,* Vol.218, pp.151 – 155.

Mukha I., Eremenko, A. M., Korchak, G. & Mikhienkova, A. (2010). Antibacterial Action and Physicochemical Properties of Stabilized Silver and Gold Nanostructures on the Surface of Disperse Silica. *J. Water Resource Protection*, Vol.2, pp.131-136.

Mukha, Yu., Eremenko, A. M. & Smirnova, N. P. (2009).Formation, physical – chemical and bactericide properties of stabilized silver nanostructures on the surface of disperse silica, *Chem., Phys.& Technol. Surf.,* Vol.15, pp. 255-266.

Nallathamby, P., Lee, K., Xu, X. (2008). Design of stable and uniform single nanoparticle photonics for *in vivo* dynamics imaging of nanoenvironments of zebrafish embryonic fluids. *ACS Nano*, Vol.2, pp.1371-1380.

Nguyen, V. &, Do, D.D. (1999). A New Method for the Characterization Of Porous Materials. Langmuir, Vol.15, pp. 3608- 3615.

Oka, H., Ikai, Y., Kawamura, N., Yamada, M., Harada, K., Ito, S., Suzuki, M. (1989). Photodecomposition products of tetracycline in aqueous solution. *J. Agric. Food Chem.*, Vol.37, pp.226-231.

Ozkaraoglu, E., Tunc, I. & Suzer, S. (2007). X-ray induced reduction of Au and Pt ions on silicon substrates. *Surf. Coat. Technol.,* Vol.201, pp.8202-8204.

Paciotti, G.F., Myer, L., Weinreich, D., Goia, D., Pavel, N., McLaughlin, R.E., Tamarkin, L., (2004). Colloidal Gold: A Novel Nanoparticle Vector for Tumor Directed Drug Delivery. *Drug Delivery*, Vol. 11, pp. 169-183.

Pal, S., Tak, Y. K., Song, J. M. (2007). Does the Antibacterial Activity of Silver Nanoparticles Depend on the Shape of the Nanoparticle? A Study of the Gram-Negative Bacterium Escherichia coli. *Appl. Environ. Microbiol.,* Vol.73, pp.1712-1720.

Paola, A., Addamo, M., Augugliaro, A., Garcia-Lopez, E., Loddo, V., Marci, G., Palmisano, L. (2004). Photolytic and TiO_2-Assisted Photodegradation of Aqueous Solutions of Tetracycline. *Fresenius Environ. bull.* Vol.13, pp.1275-1280.

Portales, H., Saviot, L., Duval, E., Fujii, M., Hayashi, S., Fatti, N., Vallee, F. (2001). Resonant raman scattering by breathing modes of metal nanoparticles. *J. Chem. Phys*., Vol. 115, pp.3444 – 3447.

Ptashko, T., Smirnova, N., Eremenko, A., Oranska, E., Huang, W. (2007). Synthesis and photocatalytic properties of mesoporous TiO_2/ZnO films with improved hydrophylisity. *Ads Sci & Technol*, Vol.25, pp.35-43.

Rodrı´guez-Ferna´ndez, J., Pe´rez-Juste, J., Mulvaney, P., Liz-Marza´n, L.M.(2005). Spatially-Directed Oxidation of Gold Nanoparticles by Au(III)-CTAB Complexes. *J. Phys. Chem. B*, Vol. 109, No. 30, pp.14257-14261.

Ruyck, H., Ridder, H., Renterghem, R., Wambeke, F. (1999). Validation of HPLC method of analysis of tetracycline residues in eggs and broiler meat and its application to a feeding trial. *Food Addit. Contam*., Vol.16, No.2, pp.47-56.

Sanniez, W.H.K., Pilpel, N. (1980). Photodecomposition of sulfonamides and tetracyclines. *J.Pharm. Sci.,* Vol.69, pp.5-8.

Schneider, S., Schmitt, M. O., Brehm, G., Reiher, M., Matousek, P., Towrie, M. (2003). Fluorescence kinetics of aqueous solutions of Tetracycline and its complexes with Mg2+ and Ca2+. Photochem. Photobiol. Sci., Vol.2, pp.1107-1117.

Sclafani, A., Mozzanega, M.N. & Herrmann, J.M. (1997). Influence of silver deposits on the photocatalytic activity of titania. *J. Catal*, Vol. 168, pp.117 – 120.

Selvan, S.T., Ono, Y., Nogami, M. (1998). Polymer-protected gold clusters in silica glass. *J. Materials Letters*., Vol. 37, pp.156 – 161.

Shacham, R., Mandler, D., Avnir, D. (2004). Electrochemically Induced Sol–Gel Deposition of Zirconia Thin Films (pages 1936–1943). J.Chem A Europ., Vol.10, pp.1936-1943.

Shi, Z.M. & Lin, L.N. (2009). Influence of La^{3+}/Ce^{3+} doping on phase transformation and crystal growth in TiO_2-15%ZnO gels. *J Non Cryst Solids*, Vol.355, pp.213-220.

Shrivastava, S., Bera, T., Roy, A., Singh, G., Ramachandrarao, P., Dash, D. (2007). Characterization of enhanced antibacterial effects of novel silver nanoparticles. *Nanotechnology,* Vol.18, pp.1-9, doi: 225103.

Shter, G.E., Behar-Levy, H., Gelman, V., Grader and, G.S., Avnir, D. (2007). Organically Doped Metals—A New Approach to Metal Catalysis: Enhanced Ag-Catalyzed Oxidation of Methanol. *Adv Function Mater.*, Vol.17, pp.913–918).

Smirnova, N., Eremenko, A., Bykovskaya, L., Kulikov, S., Chuiko, A. (1992). Fluorescence spectra of adsorbed heteroaromatic molecules at selective laser excitation *J.Molec. St.,* Vol. 266, pp. 3417 – 422.

Smirnova, N., Vorobets, V., Linnik, O., Manuilov, E., Kolbasov, G. (2010). Photoelectrochemical and photocatalytic properties of mesoporous TiO_2 films modified with silver and gold nanoparticles. *Surf. Interface Anal*., Vol.6-7, No.42, pp.1205-1208.

Song, J., Atay, T., Shi, S., Urabe, H., Nurmikko, A. (2005). Large Enhancement of Fluorescence Efficiency from CdSe/ZnS Quantum Dots Induced by Resonant Coupling to Spatially Controlled Surface Plasmons. Nano Lett., Vol.5, pp.1557-1561.

Song, Y., Nallathamby, P.D., Huang, T., Elsayed-Ali, H.E., Xu, X.H. (2010). Correlation and Characterization of 3D Morphological Dependent Localized Surface Plasmon Resonance Spectra of Single Silver Nanoparticles Using Dark-field Optical Microscopy and Spectroscopy and AFM *J. Phys. Chem. C.*, Vol.**114**, No. 1, pp. 74-81.

Subramanian, V., Wolf, E., Kamat, P. (2001). Semiconductor-Metal Composite Nanostructures. To What Extend Do Metal Nanoparticles Improve the Photocatalytic Activity of TiO_2 films? *J Phys Chem B*, Vol.105, p.11439-11448.

Sung-Suh, H., Choi, J., Hah, H., Koo, S., Bae, Y. (2004). Comparison of Ag deposition effects on the photocatalytic activity of nanoparticulate TiO_2 under visible and UV light irradiation. *J. Photochem. Photobiol. A.*, Vol. 163, pp. 37 – 44.

The Influence of Size, Shape, and Dielectric Environment. Phys.Chem.B, Vol.107, No.3, pp 668–677.

Traversa, E., Vona, M.L., Nunziante, P., Licoccia, S. (2001). Photoelectrochemical Properties of Sol-Gel Processed Ag-TiO_2 Nanocomposite Thin Films. J Sol-Gel Sci Technol., Vol.22, pp.115-123.

Vityuk, N.V., Petrik, I.S., Eremenko, A. M., Smirnova, N. P., Gorbik, P.P. (2007). Synthesis, optical and photocatalytic properties of $TiO_2/ZrO_2/SiO_2$ films modified the gold nanoparticles. *Chem. Phys. and Tech. Surf.*, Vol. 13, pp.145-151.

Vorobets, V., Manujlov, E., Smirnova, N. et al. (2008). Electro- and photocatalytic properties of electrodes based on mesoporous TiO_2-ZnO-Ag films. Chem.Phys. & Technol.Surf., Vol.14, pp.382-390.

Wang, C.T. & Lin, J.C. (2008). Surface nature of nanoparticle zinc-titanium oxide aerogel catalysts. *Appl Surf Sci*, Vol.254, pp.4500-4507.

Weaver, J.F. & Hoflund, G.B. (1994). Surface characterization study of the thermal decomposition of AgO. *J Phys Chem* Vol.98, pp.8519-8524.

Weir, E., Lawlor, A., Whelan, A., Regan, F. (2008). The use of nanoparticles in anti-microbial materials and their characterization. Analyst, Vol.133, No.7, pp.835-845.

West, J. L., Halas, N. J., (2003).Engineered Nanomaterials for Biophotonics Applications: Improving Sensing, Imaging, and Therapeutics. Ann. Rev. Biomed. Eng., Vol.5, pp.285-292.

Xin, B.F., Jing, L.Q., Ren, Z.Y. et al. (2005). Effects of simultaneously doped and deposited Ag on the photocatalyic activity and the surface states of TiO_2. *J Phys Chem B*, Vol.109, pp.2805-2809.

Yashan, G. R., Krylova, G. V. & Eremenko, A. M. (2008).Bactericide properties of gold and silver nanoparticles in solution and on high disperse silica surface, *Chem., Phys.& Technol. Surf.*, Vol. 14, pp.524- 533.

Zhang, W.F., He, Y.L., Zhang, M.S., Yin, Z., Chen, Q. (2000). Raman scattering study on anatase TiO_2 nanocrystals. *J. Phys.D: Appl.Phys.*, Vol.33, pp. 912 – 916.

Zorn, M.E., Tompkins, D.T., Zelter, W.A. et al. (2000). Catalytic and photocatalytic oxidation of ethylene on titania-based thin films. *Environ Sci Technol*, Vol.34, pp.5206–5210.

Zurhelle, G., Muller-Seitz, E., Petz, M. (2000). Automated residue analysis of tetracyclines and their metabolites in whole egg, egg white, egg yolk and hen's plasma utilizing a modified ASTED system. *J. Chromatogr. B*: *Biomed. Sci. Appl.*, Vol.739, No.1, pp.191-203.

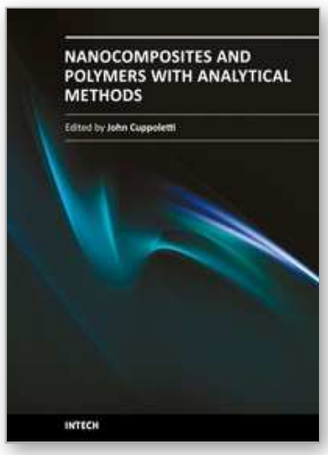

Nanocomposites and Polymers with Analytical Methods

Edited by Dr. John Cuppoletti

ISBN 978-953-307-352-1
Hard cover, 404 pages
Publisher InTech
Published online 09, August, 2011
Published in print edition August, 2011

This book contains 16 chapters. In the first part, there are 8 chapters describing new materials and analytic methods. These materials include chapters on gold nanoparticles and Sol-Gel metal oxides, nanocomposites with carbon nanotubes, methods of evaluation by depth sensing, and other methods. The second part contains 3 chapters featuring new materials with unique properties including optical non-linearities, new materials based on pulp fibers, and the properties of nano-filled polymers. The last part contains 5 chapters with applications of new materials for medical devices, anodes for lithium batteries, electroceramics, phase change materials and matrix active nanoparticles.

INTECH
open science | open minds

InTech Europe
University Campus STeP Ri
Slavka Krautzeka 83/A
51000 Rijeka, Croatia
Phone: +385 (51) 770 447
Fax: +385 (51) 686 166
www.intechopen.com

InTech China
Unit 405, Office Block, Hotel Equatorial Shanghai
No.65, Yan An Road (West), Shanghai, 200040, China
中国上海市延安西路65号上海国际贵都大饭店办公楼405单元
Phone: +86-21-62489820
Fax: +86-21-62489821

IntechOpen